Trends in Analytical Chemistry 177 (2024) 117809

Contents lists available at ScienceDirect

Trends in Analytical Chemistry

journal homepage: www.elsevier.com/locate/trac

Microfluidic immunoassays for point-of-care testing of SARS-CoV-2 antigens and antibodies

Cuili Li [a,1], Wan Zhou [b,1], Angel Gutierrez Ruiz [c], Yasaman Mohammadi [c], Qingning Li [d], Shuting Zhang [a], XiuJun Li [c,*], Guanglei Fu [a,**]

[a] School of Pharmacy, Key Laboratory of Molecular Pharmacology and Drug Evaluation, Ministry of Education, Collaborative Innovation Center of Advanced Drug Delivery System and Biotech Drugs in Universities of Shandong, Yantai University, Yantai, Shandong, 264005, China
[b] Perelman School of Medicine, University of Pennsylvania, Philadelphia, PA, 19104, USA
[c] Department of Chemistry and Biochemistry, Border Biomedical Research Center, Forensic Science, & Environmental Science and Engineering, University of Texas at El Paso, El Paso, TX, 79968, USA
[d] School of Basic Medical Sciences, Ningbo University, Ningbo, Zhejiang, 315211, China

ARTICLE INFO

Keywords:
SARS-CoV-2
COVID-19 diagnostics
Point-of-care testing
Microfluidic immunoassays
Antigens
Antibodies

ABSTRACT

The point-of-care testing (POCT) of severe acute respiratory syndrome coronavirus 2 (SARS-CoV-2) antigens and antibodies is of great significance in screening the infection and monitoring the *in vivo* immunity in controlling the pandemic. However, traditional immunoassays often require advanced laboratory settings with compromised potential in POCT. This article reviews recent advances in microfluidic immunoassays for POCT of SARS-CoV-2 antigens and antibodies. We first briefly introduce different diagnostic methods of coronavirus disease 2019 (COVID-19). After a concise introduction of different microfluidic platforms, we then focus on the latest advances in microfluidic immunoassays for POCT of SARS-CoV-2 antigens and antibodies based on different biosensing principles. In particular, some emerging biosensing principles such as photothermal biosensing are highlighted. At this end, we discuss the current challenges and future perspectives on this topic, which may shed light on new strategies on defense against similar coronavirus and other viruses to avoid pandemics in the future.

1. Introduction

The outbreak of coronavirus disease 2019 (COVID-19) has posed continuous and severe threats to public health and global economy. As of April 2024, the pandemic has led to over 7.04 million deaths worldwide reported to the World Health Organization (WHO) [1–3]. Severe acute respiratory syndrome coronavirus 2 (SARS-CoV-2) is the causing pathogen of COVID-19, which consists of a single-stranded RNA genome (~30 kb), four structural proteins (i.e., nucleocapsid (N) protein, spike (S) protein, membrane (M) protein and envelope (E) protein), and other non-structural proteins, as illustrated in Fig. 1 [4]. Although the WHO has declared the end to COVID-19 as a global public health emergency in May 2023, it does not mean that the threat from COVID-19 is over. In the past four years, SARS-CoV-2 has continuously mutated and evolved, resulting in different variants of concern (VOCs), such as Delta, Omicron and Arcturus [5]. Therefore, increasing research efforts are still in demand to control COVID-19 outbreaks, which, on the other hand, might be of significance in proactively defensing against similar coronavirus pandemics in the future.

According to different types of target biomolecules as shown in Fig. 1, three major detection methods have been developed at the molecular level, i.e., nucleic acid (i.e., RNA) test, and antigen and antibody detection, whereas the latter two employ immunoassays. Owing to the intrinsic high sensitivity and specificity, the nucleic acid amplification test (NAAT) generally serves as the "gold standard" in diagnosis of the infection by different means of technologies, such as reverse transcription-polymerase chain reaction (RT-PCR), loop-mediated isothermal amplification (LAMP), and clustered regularly interspaced short palindromic repeats and associated proteins (CRISPR/Cas) [6–10]. NAAT generally enables the detection of low copy numbers of viral RNA, which has been broadly used as a gold standard diagnostic test in the laboratory. Certain sample pre-treatment steps, including sample

* Corresponding author.
** Corresponding author.
E-mail addresses: xli4@utep.edu (X. Li), fuguanglei@ytu.edu.cn (G. Fu).
[1] Cuili Li and Wan Zhou contributed equally to the article.

https://doi.org/10.1016/j.trac.2024.117809
Received 4 May 2024; Received in revised form 4 June 2024; Accepted 4 June 2024
Available online 6 June 2024

collection, virus inactivation, nucleic acid extraction, can significantly impact the effectiveness of NAAT [11]. However, they usually require specialized laboratory infrastructures (e.g., PCR amplifiers and spectrophotometers), trained personnel and prolonged turnaround times of several hours, making them unadaptable for POCT in some extent. Immunoassays of S and/or N proteins as antigens of SARS-CoV-2 in nasopharyngeal swab samples can also test the infection, which has been widely considered as an important supplementary diagnostic method [12]. Meanwhile, immunoassays of serological antibodies to SARS-CoV-2, such as neutralizing antibodies, immunoglobulin (Ig) G and M, are capable of monitoring the *in vivo* immunity through past infection or vaccination. It is more applicable for testing the status of immunity against the virus rather than diagnosing current infection, since the antibodies are detected in delay within days to weeks after the *in vivo* immune response [13,14]. In comparison with nucleic acid tests, there is less complexity in sample preparation steps for immunoassays; antigens are also less prone to degradation as compared to RNA in terms of transport and storage; all of which allow the rapid development of immunoassays for POCT [15]. Therefore, although immunoassays provide lower sensitivity with higher possibilities of false-negative results especially when detecting at the early stage after infection, they can provide quicker results with lower cost and simpler operation. Hence, immunoassays are more suitable in a broad range of settings such as fast screening in asymptomatic people and emergent situations in large-scale outbreaks [16]. So far, various types of immunoassays, such as enzyme-linked immunosorbent assay (ELISA), fluorescence immunoassay (FIA) and chemiluminescence immunoassay (CLIA), have been developed for detecting SARS-CoV-2 antigens and antibodies [17,18]. However, some of these conventional immunoassays still have to rely on advanced analytical instruments (e.g., microplate readers) along with complicated operations, compromising their potential for POCT especially in resource-limited settings.

Microfluidic lab-on-a-chip has demonstrated substantial promise during the past decades in numerous POCT applications, such as disease diagnosis, food and drug analysis and environmental monitoring [19–26]. Due to the outstanding features, such as miniaturization, integration, low cost, and low volumes of sample and reagent consumption of the devices, various microfluidic technologies have been developed to fulfill a variety of POCT needs [27,28]. With the aid of integration with desirable biosensing principles, microfluidic immunoassays rely less on laboratory settings (e.g., bulky instruments and skilled personnel) while providing high analytical throughputs, short turnaround times and low assay costs [29]. In response to the COVID-19 pandemic, the development of microfluidic immunoassays is of particular interest for POCT of SARS-CoV-2 [30]. For example, the lateral flow immunoassay (LFIA) is a representative of those immunoassays for qualitative or semi-quantitative colorimetric detection of SARS-CoV-2 antigens, which has made a significant contribution in screening the infection in practical usage [31]. In addition, a number of other microfluidic immunoassays with various detection methods such as colorimetry, electrochemistry and fluorescence have been reported for semi-quantitative or quantitative detection of SARS-CoV-2 antigens and antibodies. Interestingly, some newly emerged principles like the photothermal biosensing have been introduced in microfluidic immunoassay of SARS-CoV-2 [32]. Various promising strategies, especially the involvement of nanomaterials, have been proposed to improve their analytical performance by amplification and/or visualization of the microfluidic detection signals [33,34]. However, it should be noted that several challenges are still encountered in this field, such as the compromised sensitivity of conventional LFIAs, requirements of additional testing accessories, and insufficient automation of devices. Therefore, it is necessary to review these most recent advances and discuss current challenges in this field. Although microfluidic methods for SARS-CoV-2 test were previously reviewed, they are mostly from different specific aspects such as nucleic acid detection or LFIA [35–38]. There are few reviews systematically focusing on microfluidic immunoassays for SARS-CoV-2 antigens and antibodies.

This article reviews recent advances in the development of microfluidic immunoassays for POCT of SARS-CoV-2 antigens and antibodies. We first briefly introduce different types of cost-effective microfluidic devices for COVID-19 from the aspect of fabrication substrates. We then focus on the latest advances in their biosensing principles. In particular, some emerging principles such as photothermal biosensing are highlighted. At the end, we discuss the current challenges and future perspectives on this topic.

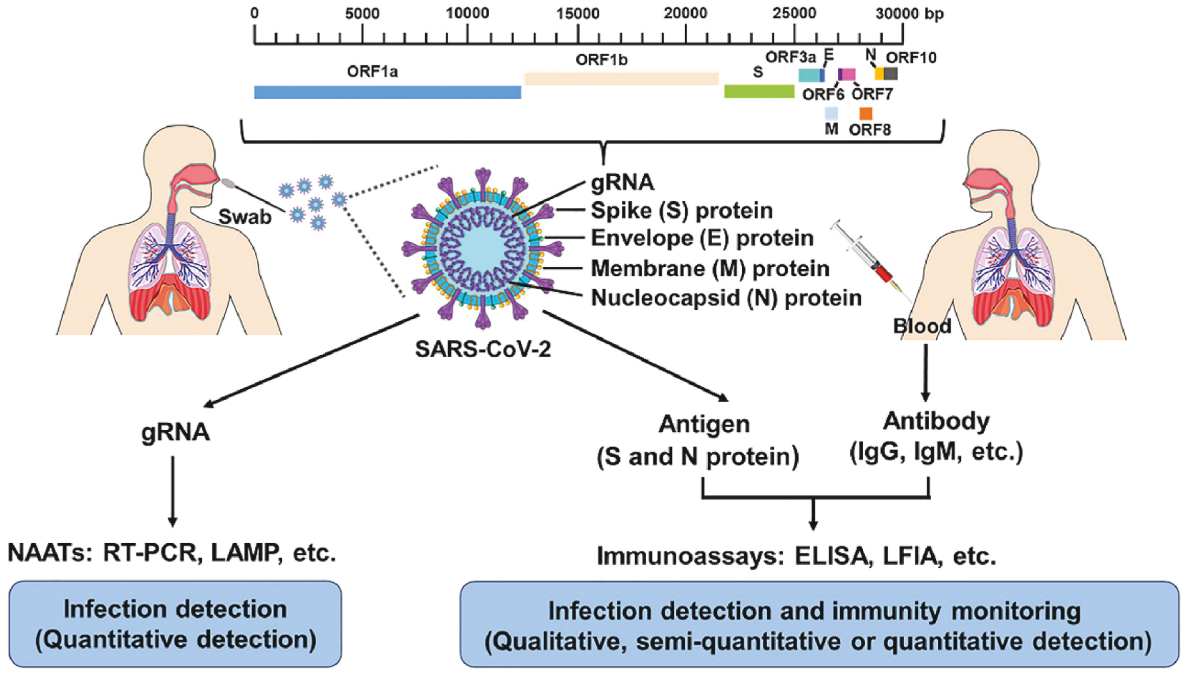

Fig. 1. Schematic summarization of detection methods for SARS-CoV-2.

2. Types of microfluidic immunoassay platforms

As one of the fundamental elements, a variety of substrate materials have been employed to fabricate microfluidic devices, such as silicon, glass, polymer and cellulose [39]. Among these materials, polymer and paper (e.g., cellulose paper and nitrocellulose (NC) membranes) substrates have attracted more attention in fabricating microfluidic devices, due to their advantages of low cost, simple manufacturing, flexibility, and versatility [28,39–42]. Based on the substrates involved, microfluidic immunoassays for SARS-CoV-2 can be categorized into three different types, namely, paper-, polymer- and hybrid material-based ones. The fabrication techniques of each type are briefly summarized in this section.

2.1. Paper-based microfluidic immunoassay platforms

Paper-based microfluidic immunoassays have shown promise in testing SARS-CoV-2 [43–45]. Using NC membranes as a key functional substrate, LFIA is a representative type that serves as a major POCT tool for SARS-CoV-2 antigens (e.g., N protein) and antibodies (e.g., IgG and IgM) in practical usage [46]. A commercial LFIA strip mainly consists of a sample pad, a conjugate pad containing gold nanoparticle-antibody conjugates, a NC membrane immobilized with specific and non-specific capture antibodies, and an absorbent pad. Due to the capillary effect, sample solutions automatically flow down the strips and interact with the nanoparticle-antibody conjugates to form immuno-complexes, followed by their immuno-capture by specific and non-specific antibodies at test and control lines, respectively. Positive or negative results are displayed as nanoparticle-induced color changes in a qualitative way [47,48]. Without any signal readers, most LFIAs can offer qualitative colorimetric results within 15–30 min. The fabrication of LFIA strips mainly involves the immobilization of antibodies/antigens and assembling of different segments, which are routine techniques and have been reviewed in previous articles [49–51].

Since the first report by Whitesides' group in 2007 [53], cellulose filter paper has been extensively employed as substrates to fabricate microfluidic paper-based analytical devices (μPADs), owing to their outstanding features, such as the three-dimensional (3D) porous microstructure, low cost, simple modification and ease of massive manufacturing [54–56]. Additionally, μPADs possess good compatibility with various biosensing modules, such as colorimetry, electrochemistry and fluorescence [57,58]. Generally, a typical μPAD is fabricated by creating hydrophilic and hydrophobic patterns as functional channels or zones for reagent-handling, molecule recognition, signal transduction and output. Common fabrication techniques on paper substrates include screen printing, origami, inkjet and wax printing and photolithography [39,59,60]. Li's group developed a microfluidic fully paper-based analytical device (μFPAD) for rapid pathogen detection with fluorescence by integrating LAMP and ssDNA-functionalized graphene oxide (GO) nano-biosensors on the chip [52]. As illustrated in Fig. 2, the device consisted of five different paper layers to construct LAMP reaction and nanosensor zones by using a simple manual photolithography technique. Since this microfluidic device was fully made of the paper substrate, it was easy to fabricate and incinerate with low costs. This was the first time to achieve LAMP reactions on a fully paper-based microfluidic device without significant reagent loss at 63 °C for a period of 1 h. After LAMP reactions, a poking-flipping actuation method was developed to transfer LAMP products to nanosensors. Based on the specific interaction between ssDNA-functionalized GO and the target LAMP products to modulate the fluorescent signals, quantitative detection of pathogens with high detection sensitivity was achieved with the limit of detection (LOD) of 6 DNA copies. Typical three-electrode arrays can be screen-printed on paper substrates to fabricate paper-based electrochemical microfluidic immunoassay devices for SARS-CoV-2. For example, Chaiyo et al. developed a paper-based electrochemical immunoassay for the serological detection of SARS-CoV-2 [61]. The functional hydrophilic channels and reaction zones were generated on paper substrates *via* wax printing to enable the capillary flow of sample liquids to the test zones. The working, reference and counter electrodes were screen-printed on the back of the paper substrates. The working electrodes were modified with GO to amplify the square wave voltammetric (SWV) signals. Li et al. presented a paper-based colorimetric microfluidic immunoassay for *anti*-SARS-CoV-2 receptor binding domain (RBD) antibodies [62]. Six parallel and discontinuous channels were fabricated by wax printing on paper substrates and were coupled with a long-arm washing segment. By rotating the washing segment, the delivery of fluids and the washing process were easily facilitated *via* the capillary effect on paper substrates.

2.2. Polymer-based microfluidic immunoassay platforms

Numerous polymer materials have been utilized as substrates in fabricating microfluidic immunoassay devices for SARS-CoV-2 [63,64]. A lot of researchers gave preference to elastomers, such as polydimethylsiloxane (PDMS), in microfluidic fabrication because of their tunable elastomeric properties, excellent transparency, high chemical inertness and compatibility with a broad range of other materials (e.g., glass) [65,66]. Photolithography and laser engraving are extensively used in prototyping and molding microfluidic patterns in PDMS substrates [67,68]. For instance, Wang et al. reported a microbubbling digital assay for testing SARS-CoV-2 recombinant N protein [69]. In the microbubbling chip, square micro-sized wells were fabricated on PDMS

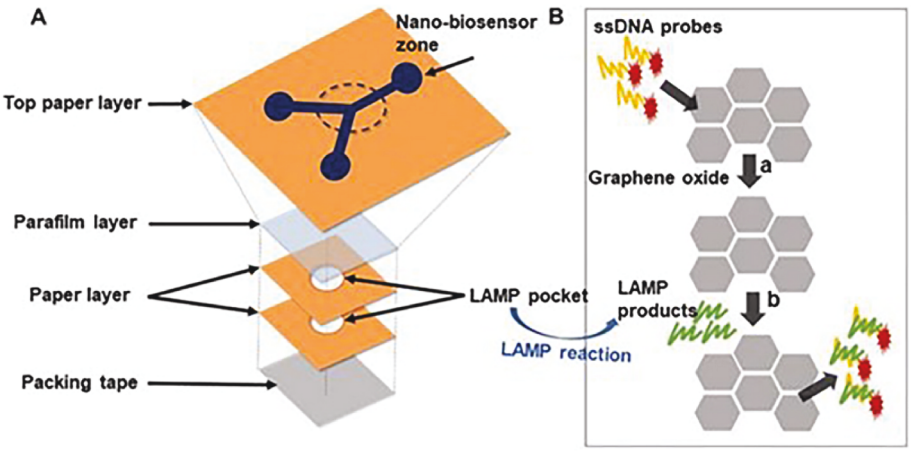

Fig. 2. Schematic of the μFPAD. (A) 3D layout of the device. (B) Pathogen detection principle based on GO nano-biosensors. Adapted with permission from Ref. [52]. Copyright 2022 Royal Society of Chemistry.

substrates *via* lithography, through which the round microbubbles generated from the immunoassay system were easily differentiated in the microwells. To enhance the airtightness and hinder the diffusion of oxygen into PDMS substrates, the microwells were modified with a layer of parylene C using the physical vapor deposition technique. Wu et al. developed a field-effect transistor (FET) sensor for SARS-CoV-2 recombinant S protein [70]. Microfluidic and electrode channels were carved in PDMS substrates by laser engraving. To optimize the channel profile, the effects of power, scanning speed and working mode of the engraving parameter were studied. After the corona treatment, the PDMS substrates were bonded with the virus-sensing transduction materials (VSTMs), two-dimensional titanium carbide (MXene)-graphene composites. Other microfabrication techniques such as inject printing and microcontact printing have been used to fabricate desirable micropatterns in PDMS substrates for other bioanalytical applications [39,41,71].

Another popular type of polymer substrates is thermoplastic materials, such as poly (methyl methacrylate) (PMMA), polyethylene terephthalate (PET) and copolymers of cycloolefin (COC). These substrates are more rigid in texture than PDMS while possessing similar features like transparency and chemical inertness, and thereby they are suitable to meet the demand in anti-deformation capability of substrates in microfluidic fabrication (e.g., supporting and slipping operations) [28]. Microfabrication methods for such substrates include computer numerical control (CNC) engraving, laser engraving, injection molding, hot embossing and 3D printing [39,72–74]. Shin et al. reported a fluorescent microfluidic chip for detecting *anti*-SARS-CoV-2 N protein IgG and IgM [75]. In the chip, two PMMA substrates were fabricated by injection molding and bonded *via* acetone injection by employing a plate pressing machine. Nanointerstices were formed at both sides of the channels during the bonding process, through which a significant pressure difference at the air-liquid interface was generated to enable the efficient sample filling. Seo et al. developed a colorimetric microfluidic immunoassay for *anti*-SARS-CoV-2 N protein antibodies [76]. Four chambers with a serpentine structure were carved in PMMA sheets by CNC engraving to serve as the reservoirs of different reagents. With the integration of passive valves to prevent the backflow of liquids, the serial injection of preserved reagents into a coil microreactor was simply implemented to undergo the immuno-reaction.

2.3. Hybrid material-based microfluidic immunoassay platforms

In recent years, hybrid material-based microfluidic devices have attracted increasing interests for POCT applications. By assembling diverse types of substrates (e.g., papers and PDMS) into a single device, their advantages in different aspects, such as biomolecule immobilization, reagent handling and fabrication of sensing elements (e.g., electrodes), can be combined [24,41,77,78]. For instance, paper/polymer hybrid devices can enable multiplexed sampling through operations like slipping of polymer segments while maintaining the ease in biomolecular immobilization in paper substrates [41,71,79,80]. PDMS has been utilized as the spraying agent to produce hydrophobic barriers in paper substrates to increase the shelf life of the devices [81]. The fabrication of hybrid microfluidic devices usually involves the assembly of different segments, such as embedding papers into polymeric chambers, sealing and bonding among different substrates. McDevitt et al. fabricated a hybrid microfluidic device for the fluorescent detection of *anti*-SARS-CoV-2 RBD antibodies [82]. Hydrophilic adhesive was bound with a PMMA sheet to act as the bottom substrate of the chip. In the substrate, the adhesive facilitated the flow of sample liquids into a cartridge *via* capillary effect. The immuno-reaction and display of fluorescence signals took place in an array of hexagon-shaped detection wells in the cartridge. Table 1 summarizes features of different substrate materials in microfluidic immunoassay platforms, including advantages and disadvantages of them in operation, fabrication, and performance.

Table 1
Summarization of features of different substrates in microfluidic immunoassay platforms.

Microfluidic immunoassay platforms	Substrate materials	Advantages	Disadvantages
Paper-based	NC membrane	Ease of biomolecule immobilization, simple assembly, and flexibility	Low mechanical strength and low performance in flow control and reagent delivery
	Cellulose paper	Low cost, 3D porous structure for easy reagent storage and reaction, ease of massive manufacturing, flexibility, and disposability	Nonuniform porous structure, low performance in flow control and reagent delivery, low mechanical strength, and low repeatability
Polymer-based	Thermoelastomers (PDMS)	Tunable elastomeric properties, excellent transparency, gas permeability, high performance in flow control and reagent delivery, and rapid prototyping & molding of patterns	Prone to deformation, absorbing & releasing of biomolecules and requirement of cleanroom facility for high-resolution fabrication
	Thermoplastic (PMMA, PET and COC)	Excellent transparency, high chemical inertness, anti-deformation, rapid prototyping, high repeatability, and high performance in optical detection	Requirement of high temperature or energy in fabrication and low resolution
Hybrid material-based	paper/PDMS, paper/PMMA, etc.	Combined features of hybrid materials: ease of biomolecule immobilization, high performance in flow control and reagent delivery, versatility, and flexibility	Requirement of more efforts to integrate different substrates in massive manufacturing

3. Biosensing principles and applications of microfluidic immunoassays

Various biosensing principles have been integrated into diverse types of microfluidic devices to develop immunoassays for SARS-CoV-2, which have shown considerable promise in POCT. From the aspect of immunologic recognition principle, recognition elements including antibodies, antigens and aptamers play a basic role in constructing these microfluidic immunoassays. On the other hand, the detection principles such as colorimetry, fluorescence, chemiluminescence, electrochemiluminescence, surface-enhanced Raman scattering, and electrochemistry are of broad interest in this field [18,47,83,84]. In this section, we focus on these recent advances in the biosensing principle from the two aspects above in these microfluidic immunoassays for SARS-CoV-2 antigens and antibodies.

3.1. Immunologic recognition elements

Generally, the microfluidic immunoassays for SARS-CoV-2 are based on the immunologic recognition between SARS-CoV-2 antigens (e.g., structural proteins) and their antibodies (e.g., Ig G and Ig M). These recognition elements are used as either the immuno-capture elements or

targets in different cases. Because of the specificity in recognizing the virus, S and N proteins are extensively selected as the antigens in these works. For example, Chen et al. developed a microfluidic particle counter for visual detection of *anti*-SARS-CoV-2 RBD antibody in nasal secretions [85]. Magnetic microparticles (MMPs)-labeled RBD antigen and polystyrene microparticles (PMPs)-labeled anti-human IgG were used to establish the immunologic recognition system, respectively. In the presence of the target *anti*-SARS-CoV-2 RBD antibody, MMPs bound with PMPs. After magnetic separation, free PMPs were loaded into the particle counter to read their accumulation length in a trapping channel. The LOD of *anti*-SARS-CoV-2 RBD antibody was 14.0 ng/mL. Zhou et al. reported a LFIA for fast and sensitive determination of SARS-CoV-2 N protein in nasal swab samples using surface structure membrane (SS Mem) as a lateral-flow membrane [86]. A traditional sandwich-type recognition system between SARS-CoV-2 N protein and its antibodies (i.e., capture and probe-labeled detection) was constructed on the SS Mem. Taking advantage of the SS Mem for fast self-transport of sample solutions with convection and low residual, the LFIA enables the colorimetric and fluorescent detection of the target with LODs of 3.98 pg/mL and 53.3 fg/mL, respectively. Liu et al. integrated μPADs with a centrifugal microfluidic disc for colorimetric immunoassay of SARS-CoV-2 N protein in saliva samples [87]. They constructed a sandwich-type recognition system in detection wells of the μPADs using Au NPs as the colorimetric probe. Using the centrifugal disc for sample separation and reagent delivery, N protein was tested at the LOD of 10 pg/mL. In addition, Chai et al. presented a digital microfluidic (DMF) platform for fluorescent detection of SARS-CoV-2 N protein in saliva using aggregation-induced emission fluorgens (AIEgens) [88]. Magnetic beads and AIEgnes with high fluorescent intensity and photostability were employed to label the capture and detection antibodies, respectively, to establish the sandwich-type recognition system with the aid of droplets generated in the chip. The LOD of N protein was as low as 5.08 pg/mL.

Besides the direct immunologic recognition between antibodies and antigens, aptamers are also an important alternative to construct the recognition system for microfluidic immunoassay of SARS-CoV-2. For instance, Li et al. reported an aptamer/antibody sandwich method for digital detection of SARS-CoV-2 N protein in serum samples [89]. Magnetic beads (MBs) and β-galactosidase (β-Gal) were utilized to label the capture antibody and detection aptamer, respectively, to construct the sandwich-type recognition system. The conjugates were loaded into a microfluidic chip to measure the number of fluorescent femtoliter-sized wells. The LOD of SARS-CoV-2 N protein was 33.28 pg/mL. Trakht et al. proposed a microfluidic enrichment strategy for fluorescent detection of SARS-CoV-2 viral particles in nasal swab samples [90]. Aptamers with two different spike domains (i.e., RBD and *N*-terminal domain) were employed as the capture elements in the recognition system in a herringbone microfluidic chip, through which the resistance to mutated strains of the virus can be improved. Fluorescent signals were generated by the hydrolysis of beta-galactosidase (β-Gal), and the LOD was as low as 37 active virions/μL. Pun et al. reported an aptamer-based colorimetric LFIA for SARS-CoV-2 S protein in nasal swab samples using Au NPs as the probe [91]. A new sequence, namely SARS-CoV-2 spike protein NTD-binding DNA aptamer 4 (SNAP4), was discovered and used as the capture element to construct the sandwich-type recognition system using SNAP1 to label the detection probe (Au NPs).

3.2. Detection principles and applications

In addition to conventional detection principles such as colorimetry, fluorescence, chemiluminescence, electrochemiluminescence, surface-enhanced Raman scattering, and electrochemistry, some newly emerged principles like the photothermal biosensing are also applied for microfluidic immunoassay of SARS-CoV-2 antigens and antibodies [32,92–95]. Strategies such as signal amplification and visualization in microfluidic devices are proposed to improve the immunoassay performance or potential in POCT. For instance, nanomaterials (e.g., nanoparticles (NPs)) are widely exploited in these works to modulate the analytical signals [96]. We discuss LFIAs separately in each principle because of their unique potential in POCT especially in practical applications. Recent advances of microfluidic immunoassays for SARS-CoV-2 detection with their key analytical parameters are summarized in Table 2.

3.2.1. Colorimetry detection

Colorimetry has emerged as one of the most popular detection principles in microfluidic immunoassays for SARS-CoV-2, ascribed to the ease of visual signal readout without relying on sophistical analytical instruments [97]. In order to improve the analytical performance (e.g., sensitivity), the physical and chemical properties of nanomaterials, such as the plasmonic properties and catalytic activities, are widely applied to transduce or amplify the colorimetric signals [98,99]. The exploitation of NPs such as noble metal and metal oxide NPs as peroxidase mimics to catalyze the chromogenic reaction of 3,3′,5,5′-tetramethylbenzidine (TMB) is a typical example [93,100]. With the aids of image-analyzing approaches, such as the measurement of gray value, microfluidic immunoassays can provide quantitative detection results [97,98].

One of the representative colorimetric microfluidic immunoassays is the gold NPs-based LFIAs, which have been developed commercially for testing SARS-CoV-2 antigens in practical usage [101]. It should be noted that conventional LFIAs are more suitable for qualitative detection, i.e., by only providing positive or negative results. Attributed to the colorimetric working principle, the sensitivity of LFIAs is usually compromised, which might lead to false-negative detection results. Recently, some strategies have been applied to LIFAs either to improve the sensitivity or to enable quantitative results for SARS-CoV-2 immunoassays. For example, Kim et al. developed a colorimetric LFIA for SARS-CoV-2 N protein in saliva samples using plasmon color-preserved Au nanoclusters as the probe [102]. Au nanoclusters with nanogaps were synthesized *via* the streptavidin-biotin binding among Au NPs, through which the plasmon coupling among NPs was avoided to improve the colorimetric sensitivity. The nanoclusters maintained the intrinsic plasmonic properties of Au NPs with enhanced light absorption. By using an optical reader, the LOD of N protein was as low as 38 pg/mL, which was 5.9 times lower than that using Au NPs of the same size. Chaiyo et al. developed a self-enhancement colorimetric LFIA for SARS-CoV-2 N protein in saliva samples [97]. Different from the conventional LFIAs, an enhancing pad was additionally added in the strip where Au^{3+} and reducing agent (HA) were reserved. When sample solutions infiltrated from the conjugate pads to the enhancing ones, enlarged Au NPs were formed *via* the reaction between Au^{3+} and HA, resulting in enhanced color changes and improved detection sensitivity. The assay detected N protein at LODs of 0.5 and 0.1 ng/mL with the naked eye and readout of grayscale value of the detection regions, respectively. Kim et al. presented a colorimetric LFIA based on using a bifunctional fusion linker, CBP31-BC, for antibody immobilization in the detection of RBD of SARS-CoV-2 S protein and inactivated SARS-CoV-2 in nasopharyngeal swab samples [47]. The usage of the linker enabled the immobilization of capture antibodies in cellulose membranes (i.e., test lines) in an oriented manner and achieved the colorimetric assay by binding Au NPs-conjugated detection antibodies. The LODs for RBD antigen and inactivated SARS-CoV-2 were 0.63 ng/mL and 5×10^4 copies/mL, respectively, with 100 % accuracy in testing 19 clinical samples. Using aptamers to *N*-terminal domain (NTD) of S protein, Pun et al. developed a sandwich-type LFIA for SARS-CoV-2 S protein in nasal swab samples [91]. As shown in Fig. 3A, two oligonucleotide aptamers with high affinity were synthesized and employed as the capture and detection ligands, respectively, to construct the sandwich-type assay system in the colorimetric LFIA strip. The LFIA strips were finally immersed into enhancing buffers containing Au^{+} to enlarge the size of captured Au NPs, through which the colorimetric signals were

Table 2
Summarization of recent advances in microfluidic immunoassays for SARS-CoV-2 antigens and antibodies using various biosensing principles.

Principle	Device substrate	Target	Recognition elements	Label materials	Linear range	LOD	Ref.
Colorimetry	NC membrane	N protein	Capture element: *anti*-N protein antibody; Detection element: *anti*-N protein antibody	Au nanoclusters	300 pg/mL-1000 ng/mL	38 pg/mL	[102]
Colorimetry	NC membrane	N protein	Capture element: *anti*-N protein antibody; Detection element: *anti*-N protein antibody	Au NPs	0.5–2000 ng/mL	0.5 ng/mL (with naked eye); 0.1 ng/mL (measurement of gray value)	[97]
Colorimetry	NC membrane	RBD antigen; Inactivated virus	Capture element: *anti*-S protein antibody; Detection element: *anti*-S protein neutralizing antibody	Au NPs	— —	0.63 ng/mL; 5.0×10^4 copies/mL	[47]
Colorimetry	NC membrane	S protein	Capture element: S protein NTD-binding DNA aptamer 4; Detection element: S protein NTD-binding DNA aptamer 1	Au NPs	—	500 pM	[91]
Colorimetry	NC membrane	*Anti*-N protein IgG; *Anti*-N protein IgM	Capture element: anti-human IgG and anti-human IgM; Detection element: recombinant N protein	Se NPs	5–200 ng/mL; 20–200 ng/mL	5.0 ng/mL; 20 ng/mL	[103]
Colorimetry	Resin	N protein	Capture element: *anti*-N protein antibody; Detection element: *anti*-N protein antibody	HRP	—	54 pg/mL (in buff); 91 pg/mL (in diluted saliva)	[104]
Colorimetry	Paper	*Anti*-RBD IgG; *Anti*-RBD IgM; *Anti*-RBD IgA	Capture element: RBD antigen; Detection element: anti-human IgA, anti-human IgM, and anti-human IgG	HRP	0–100 ng/mL; 0–100 ng/mL; 0–100 ng/mL	1.25 μg/mL; 0.5 μg/mL; 1.25 μg/mL	[62]
Colorimetry	Cellulose paper	N protein	Capture element: SsoNP.E2-CBD; Detection element: biotinylated MBP-SsoNP.E1	HRP	—	3.8 ng/mL (in mock swab); 1.9 ng/mL (in saliva)	[105]
Colorimetry	PMMA	Neutralizing antibody	Capture element: RBD antigen; Detection element: anti-human IgG	HRP	10–1000 ng/mL	—	[98]
Colorimetry	Glass/PDMS	*Anti*-N protein antibody	Capture element: recombinant N protein; Detection element: anti-rabbit IgG	HRP	2.17 pg/mL-21.7 ng/mL	4.14 pg/mL (LOQ)	[107]
Colorimetry	Glass/PDMS	Inactivated virus	Capture element: *anti*-N protein antibody; Detection element: *anti*-N protein antibody	Red polystyrene nanobeads	—	100 copies/mL	[108]
Colorimetry	PMMA/PDMS	N protein	Capture element: *anti*-N protein antibody; Detection element: *anti*-N protein antibody	Au@Pt NPs	—	10 pg/mL (with naked eye); 0.1 pg/mL (measurement of absorbance)	[109]
Fluorescence	NC membrane	S protein	Capture element: *anti*-S protein antibody; Detection element: *anti*-S protein antibody	SiO_2@Au/QD nanocomposites	—	0.033 ng/mL	[83]
Fluorescence	NC membrane	Neutralizing antibody	Capture element: anti-human IgG and IgM; Detection element: recombinant RBD antigen	Eu chelate NPs	12.5–1000 IU/mL	7.6 IU/mL	[118]
Fluorescence	NC membrane	*Anti*-S protein IgM; *Anti*-S protein IgG	Capture element: anti-human IgM and anti-human IgG; Detection element: recombinant S protein	Aggregation-induced emission PS NPs	— —	0.236 μg/mL; 0.125 μg/mL	[96]
Fluorescence	Paper	*Anti*-RBD IgG	Capture element: *anti*-RBD antibody; Detection element: RBD antigen	PS particle	1.0–50 ng/mL	1.0–5.0 ng/mL	[119]
Fluorescence	Paper	Inactivated virus	Capture element: — Detection element: *anti*-N protein antibody	PS particle	0–800 pg/mL	—	[121]
Fluorescence	Polycarbonate	N protein; *Anti*-S protein IgG	Capture element: *anti*-N protein antibody and anti-human IgG; Detection element: *anti*-N protein antibody and S protein	FMSs	0.15−150 ng/mL; 1.0−100 ng/mL	0.85 ng/mL; 5.80 ng/mL	[122]

(*continued on next page*)

Table 2 (*continued*)

Principle	Device substrate	Target	Recognition elements	Label materials	Linear range	LOD	Ref.
Fluorescence	PMMA/PDMS	*Anti*-RBD antibody	Capture element: RBD antigen; Detection element: anti-human IgG or IgM	PE	—	1.6 ng/mL	[63]
CL	NC membrane	S protein	Capture element: *anti*-S protein antibody; Detection element: *anti*-S protein antibody	Co–Fe@hemin-peroxidase nanozymes	0.2–100 ng/mL	0.1 ng/mL	[18]
SERS	NC membrane	*Anti*-S protein IgG; *Anti*-S protein IgM	Capture element: anti-human IgM and anti-human IgG; Detection element: S protein	DTNB-loaded SiO_2@Ag NPs	— —	1.0 pg/mL; 1.0 pg/mL	[136]
SERS	NC membrane	*Anti*-S protein IgG	Capture element: S protein; Detection element: anti-human IgG	Ag^{MBA}@Au	10^{-9}-10^{-4} mg/mL	0.22 pg/mL (in buff); 0.52 pg/mL (in serum)	[139]
SERS	NC membrane	N protein	Capture element: *anti*-N protein antibody; Detection element: *anti*-N protein antibody	Au^{MGITC} NPs	—	3.53 PFU/mL	[84]
SERS	NC membrane	*Anti*-S and N protein IgG; *Anti*-S and N protein IgM	Capture element: anti-human IgM and anti-human IgG; Detection element: S and N protein	GERTs	— —	1.0 ng/mL; 0.1 ng/mL	[140]
SERS	Glass/PDMS	N protein	Capture element: *anti*-N protein antibody; Detection element: *anti*-N protein antibody	Hollow gold nanospheres	6.0–100 PFU/mL	0.22 PFU/mL	[137]
SERS	Glass/PDMS	*Anti*-S protein antibody	Capture element: S protein; Detection element: —	Gold nanospikes	—	0.5 pM	[141]
Electrochemistry	Paper	*Anti*-RBD IgG; *Anti*-RBD IgM	Capture element: RBD antigen; Detection element: —	HRP	1–1000 ng/mL; 1–1000 ng/mL	0.96 ng/mL; 0.14 ng/mL	[61]
Electrochemistry	Polyester	*Anti*-N protein IgG	Capture element: N protein; Detection element: anti-mouse IgG	HRP	—	5.0 ng/mL	[148]
Electrochemistry	PMMA	N protein	Capture element: *anti*-N protein antibody; Detection element: *anti*-N protein antibody	DMBs	0–10 ng/mL	50 pg/mL (in serum); 10 pg/mL (in 5-fold diluted serum)	[72]
Electrochemistry	PMMA	N protein	Capture element: *anti*-N protein antibody; Detection element: —	$[Fe(CN)_6]^{3-/4-}$	10–1000 pg/mL	3.1 pg/mL	[64]
Electrochemistry	Polyester/ resin	*Anti*-N protein IgG; *Anti*-S protein IgG	Capture element: N protein and S protein; Detection element: anti-human IgG	Alkaline phosphatase	30–750 ng/mL; 20–1000 ng/mL	28 ng/mL; 15 ng/mL	[150]
Electrochemistry	Glass/PDMS	*Anti*-S1 protein antibody; *Anti*-RBD antibody	Capture element: S1 protein and RBD antigen; Detection element: —	—	— —	2.8×10^{-15} M; 16.9×10^{-15} M	[152]
Photothermal biosensing	NC membrane	*Anti*-S protein IgG	Capture element: anti-human IgG; Detection element: S protein	$ReSe_2$ nanosheets	1.0 ng/mL-10 μg/mL	0.86 ng/mL	[34]
Photothermal biosensing	NC membrane	RBD antigen	Capture element: *anti*-RBD antibody; Detection element: *anti*-RBD antibody	Gold nanosphere	—	0.45 aM (in buff); 3.6 aM (in nasopharyngeal wash)	[162]
Photothermal biosensing	NC membrane	*Anti*-RBD antibody	Capture element: RBD antigen; Detection element: anti-human antibody	Au NPs	—	0.1 μg/mL	[32]
Distance-based detection	PE	N protein	Capture element: —; Detection element: *anti*-N protein antibody	Red latex nanobeads	1.0–10 μg/mL	1.0 μg/mL	[166]
Distance-based detection	Paper	N protein	Capture element: —; Detection element: *anti*-N protein antibody	PS article	—	1.0 fg/mL (in saliva); 10 fg/mL (in simulated saline gargle)	[167]
Distance-based detection	Glass/PDMS	*Anti*-RBD antibody	Capture element: RBD antigen; Detection element: anti-human IgG	PMP	5.0–1000 ng/mL (sensitive mode); 50–3000 ng/mL (rapid mode)	13.3 ng/mL; 57.8 ng/mL	[157]

Abbreviations: CL, chemiluminescence; SERS, surface-enhanced Raman scattering; NC, nitrocellulose; PMMA, methyl methacrylate; PDMS, polydimethylsiloxane; PE, Polyethylene; N protein, nucleocapsid protein; S protein, spike protein; RBD antigen, receptor binding domain antigen; Ig, immunoglobulin; NTD, *N*-terminal domain; CBD, cellulose-binding domain; MBP, maltose-binding protein; SsoNP.E1, selected reporter binder; NP, nanoparticles; HRP, horseradish peroxidase; Au@Pt, platinum-decorated gold; QD, quantum dot; PS, polystyrene; FMS, fluorescent carboxylate-modified microparticles; PE, phycoerythrin; DTNB, 5,5-dithiobis-(2-nitrobenzoic acid); MBA, 4-mercaptobenzoic acid; MGITC, malachite green isothiocyanates; GERT, gap-enhanced Raman tags; DMB, dually-labeled magnetic nanobeads; $ReSe_2$, rhenium diselenide; PMP, polystyrene microparticles; LOD, limit of detection; LOQ, limit of quantification.

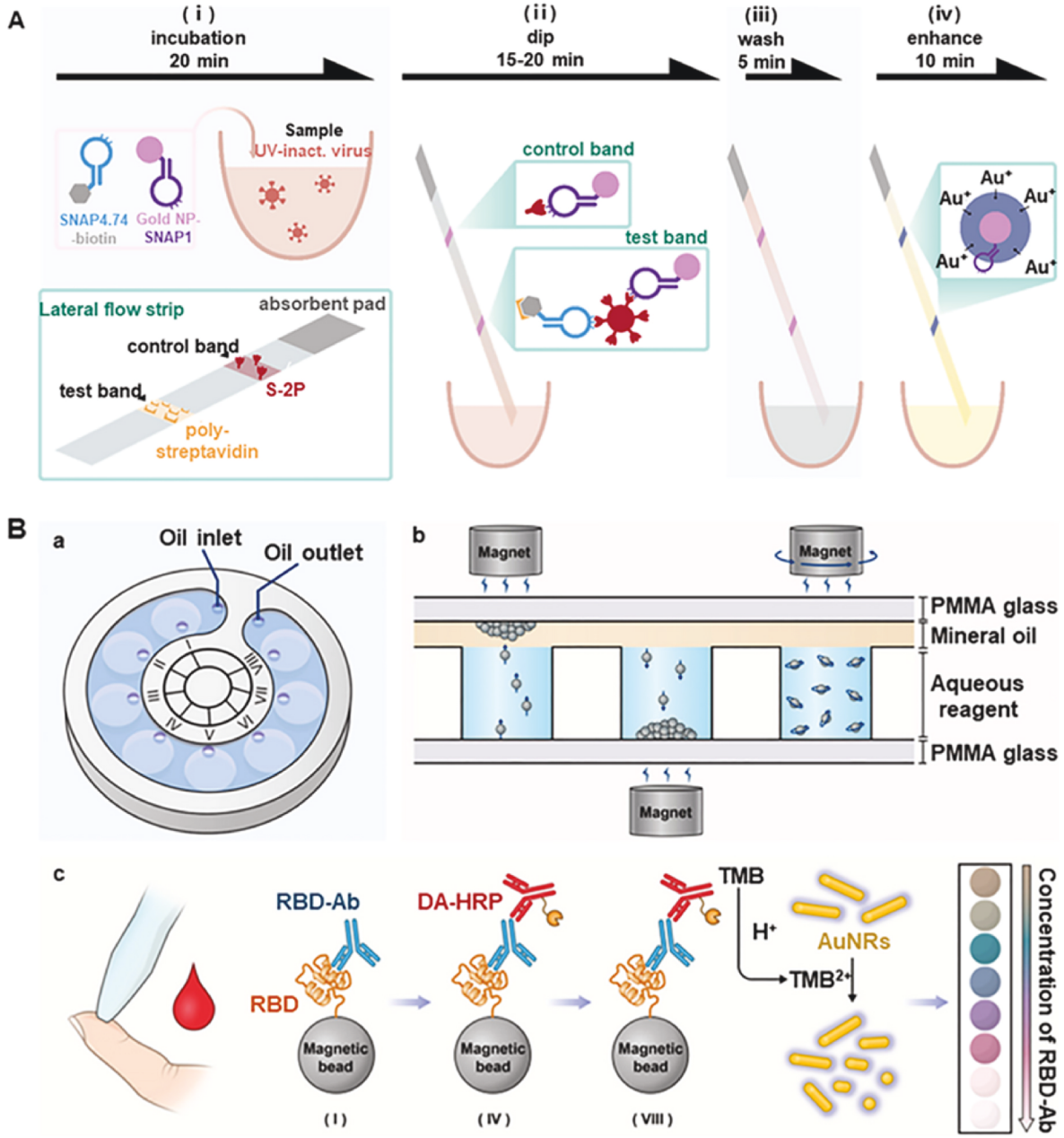

Fig. 3. Colorimetric microfluidic immunoassays for SARS-CoV-2. (A) Scheme of the colorimetric LFIA for SARS-CoV-2 S protein based on using NTD aptamers and enhancing buffers for signal amplification. Adapted with permission from Ref. [91]. Copyright 2022 American Chemical Society. (B) Scheme of the magnetofluid-integrated multicolor chip for colorimetric immunoassay of SARS-CoV-2 neutralizing antibody. (a) 3D layout of the microfluidic chip. (b) Illustration of magnet-manipulated movement of beads between two phases (i.e., oil and aqueous solutions) in the chip. (c) Colorimetric immunoassay principle based on the etching of Au nanorods. Adapted with permission from Ref. [98]. Copyright 2022 American Chemical Society.

amplified. The assay could detect as low as 500 pM S–2P protein spiked in normal nasal swab samples. In addition, Ma et al. reported a colorimetric LFIA for *anti*-SARS-CoV-2 N protein IgM and IgG in serum and blood using Se NPs as the colorimetric probe [103]. Se NPs-labeled N protein could specifically bind with IgG and IgM at test lines, displaying an orange color that was positively related with the concentrations of the targets. It was concluded that the simultaneous detection of IgM and IgG could improve the detection accuracy, as it not only responded to early infection but also indicated previous infection. IgG and IgM were quantified at LODs of 5.0 ng/mL and 20 ng/mL, respectively.

Owing to distinct merits of μPADs in POCT, the colorimetric principle has been extensively integrated into μPADs and relevant hybrid devices for immunoassays of SARS-CoV-2 antigens and antibodies. Juncker et al. developed a 3D-printed resin/paper hybrid colorimetric immunoassay for SARS-CoV-2 N protein in saliva [104]. A capillary aliquoting circuit was fixed in the microfluidic chip to discharge excessive liquids and avoid precise pipetting. By click-connecting the prime capillary pump to the chip, the sandwich immuno-reaction and washing procedures were performed sequentially and automatically. Brown precipitates were generated from the oxidation of 3,3′-diaminobenzidine (DAB) in the presence of immuno-captured horseradish peroxidase (HRP). The LOD for N protein in diluted saliva samples was 91 pg/mL. Li's group integrated a pulling-force spinning top (PFST) into a paper-based microfluidic chip for colorimetric immunoassay of *anti*-SARS-CoV-2 RBD antibodies in serum [62]. Finger blood was obtained by capillary siphoning and centrifugally separated by the PFST. Plastic

comb binding spines served as switches to control the liquid flow in the chip. HRP-labeled detection antibody was used to establish an indirect immunoassay system in the paper chip utilizing DAB as the chromogenic substrate. IgG, IgM and IgA were tested at LODs of 1.25 μg/mL, 0.5 μg/mL and 1.25 μg/mL, respectively, indicating that the detection sensitivity were not very high. Sikes et al. fabricated a vertical-flow paper-based microfluidic chip for immunoassay of SARS-CoV-2 N protein in saliva based on rapid affinity pair identification *via* directed selection (RAPIDS) [105]. Compared with the conventional lateral flow, the vertical flow of sample liquids through multiple layers of papers decreased the influence of non-specific immuno-binding ascribed to the low linear flow rate. Hence, the background colorimetric signals were reduced because large particles were filtered during the flow process. In addition, the RAPIDS could screen high affinity pairs for N protein to improve the sensitivity. N protein in mock swab and saliva samples was quantified with LODs of 3.8 ng/mL and 1.9 ng/mL, respectively.

Polymer-based and relevant hybrid microfluidic devices are also widely employed for colorimetric immunoassays of SARS-CoV-2. As a typical example, these devices leveraged the color changes of specific chromogenic substrates like TMB. For instance, Zhu et al. developed a magnetofluid-integrated multicolor immuno-chip (MMI-chip) for colorimetric immunoassay of SARS-CoV-2 neutralizing antibody in serum [98]. As shown in Fig. 3B, magnetic beads-labeled RBD antigen and HRP-labeled IgG were used as the capture and signaling elements in the immuno-recognition system, respectively. The MMI-chip had a 3D two-phase liquid layout, through which different aqueous reagents in vertical chambers were blocked by an upper oil layer and the immuno-reaction process was implemented by moving immuno-complexes in these reagents using a magnet. The oxidation of TMB facilitated the etching of Au nanorods to display sensitive colorimetric signals, as previously reported by the Li group [106]. This microfluidic immunoassay showed 100 % specificity and 83.3 % sensitivity in testing real serum samples from vaccine-immunized volunteers. Zhou et al. presented a glass/PDMS hybrid microfluidic chip for immunoassay of *anti*-SARS-CoV-2 N protein antibodies based on reciprocating-flowing (RF) immuno-binding [107]. In contrast to the static immuno-binding *via* free diffusion, the integrated RF protocol achieved repeated contact between antibodies and N proteins on PDMS substrates with a short binding runtime of less than 2.0 min. Using TMB as the chromogenic substrate, the antibody was determined at a limit of quantification (LOQ) of 4.14 pg/mL through analyzing gray value of images of the detection regions. Lao et al. presented a handheld microfluidic filtration platform for colorimetric immunoassay of inactivated SARS-CoV-2 in swab samples [108]. White microbeads and red nanobeads were used to label two types of noncompetitive *anti*-N protein antibodies, respectively, to form immuno-complexes, followed by their injection into a PDMS chip where only larger immuno-complexes were retained by a blocking column array in the filtration segment. As a result, red colorimetric signals were produced in the central observation zones in the presence of target N protein. The microfluidic test kit could detect inactivated SARS-CoV-2 viral particles at a LOD of less than 100 copies/mL. Ma et al. exploited platinum-decorated gold (Au@Pt) NPs as peroxidase mimics to develop a PDMS colorimetric microfluidic immunoassay for SARS-CoV-2 N protein in throat swab samples [109]. Magnetic beads and Au@Pt NPs with high catalytic activity were used to label the capture and detection antibodies, respectively, to establish the multiplexed immunoassay system. In the chip, rubber plugs were employed to release reagents and washing buffers in the immuno-reaction process with the aid of an external magnet for sample separation. This method exhibited excellent detection sensitivity. Using TMB as the chromogenic substrate, the LOD of N protein was as low as 0.1 pg/mL.

3.2.2. Fluorescence detection

Fluorescence detection has been extensively applied in microfluidic immunoassays for SARS-CoV-2 antigens and antibodies [110,111]. The detection sensitivity of fluorescence is generally higher than that of some other optical methods such as the colorimetry [77,112]. At present, portable fluorescence readers are commercially available, enhancing the potential of such assays in POCT. In addition, some image-analyzing approaches can be used to quantitatively analyze the fluorescent signals for quantitative detection. Fluorophores such as quantum dots (QDs) and organic dyes are popular fluorescent probes in microfluidic immunoassays [17]. Strategies like nanomaterial-mediated fluorescence amplification and quenching are widely exploited to improve the analytical performance [83,113].

Fluorescent probes can be integrated into LFIAs for qualitative or quantitative immunoassays of SARS-CoV-2 [114,115]. By analyzing gray value of fluorescent images or using optical strip readers, quantitative detection can be realized as the colorimetric detection does. Xiao et al. developed a LFIA for quantification of SARS-CoV-2 S protein in saliva using SiO_2@Au/QD nanocomposites as the fluorescent probe [83]. The nanocomposites were prepared by successively synthesizing Au NPs and QDs on surfaces of SiO_2 nanocores, which could significantly improve the coupling efficiency and amplify the fluorescent signals. The LOD of this assay for S protein was as low as 0.033 ng/mL. The analytical recoveries of the determination of S protein in spiked saliva samples ranged from 93.63 % to 98.02 %, demonstrating a satisfactory accuracy of the assay in the detection. Compared with IgM or IgG, the detection of total *anti*-SARS-CoV-2 antibodies in serum are considered more sensitive for early diagnosis of the infection [116]. Xiong et al. reported a fluorescent LFIA for testing total SARS-CoV-2 antibodies in serum using quantum dot nanobeads (QBs) as the probe [117]. In this work, plenty of QDs were embedded in a polycarbonate substrate to produce the high luminescent QBs, followed by the covalent linking of recombinant SARS-CoV-2 S proteins to construct a double-antigen sandwich-type immunoassay system for total antibodies. Owing to the high fluorescent intensity of QBs, the sensitivity of the assay was one order of magnitude higher than that of conventional Au NPs-based LFIA. In addition, the detection was achieved rapidly within 15 min without the need of any bulky and advanced instruments. Jiang et al. integrated Eu chelate NPs as the fluorescent probe in a LFIA for the quantitative detection of *anti*-SARS-CoV-2 neutralizing antibodies using the ratiometric fluorescence analysis [118]. The authors justified that the ratiometric fluorescence method was less commonly used in immunochromatographic assays, but it was more sensitive and accurate than single-signal measurements that were susceptible to various external factors. The assay was able to detect neutralizing antibodies at a LOD of 7.6 IU/mL and could discriminate different concentrations in the range of 12.5–1000 IU/mL. Li et al. developed a fluorescent LFIA for the simultaneous detection of *anti*-SARS-CoV-2 IgM and IgG in clinical serum samples [96]. Near infrared-emissive aggregation-induced emission molecules were bonded to surfaces of polystyrene (PS) NPs *via* the organic solvent swelling method to avoid the interference of autofluorescence. This method allowed for more sensitive detection of IgM and IgG at earlier infection stages than the conventional Au NPs-based LFIAs. Under optimal conditions, the LODs of IgM and IgG were 0.236 μg/mL and 0.125 μg/mL, respectively.

Fluorescence detection has been widely exploited in μPADs and related hybrid devices for the immunoassay of SARS-CoV-2, given the ease of constructing ELISA systems in paper substrates [43]. Yoon et al. presented a paper-based fluorescent competitive microfluidic immunoassay for *anti*-SARS-CoV-2 IgG in clinical saline gargle samples [119]. Saliva testing offers non-invasive and easy operation, but it usually requires high sensitivity because of the presence of trace contents of antibodies in saliva. As shown in Fig. 4A, *anti*-SARS-CoV-2 RBD antibody was immobilized in test zones of the paper chip through the supramolecular interaction. In the simultaneous presence of immobilized *anti*-RBD antibody and free IgG, PS particle-labeled RBD antigen tended to conjugate with the latter one in a competitive manner. The assay signals were monitored by counting the immuno-captured luminescent particles in the test zones or evaluating the capillary flow velocities of

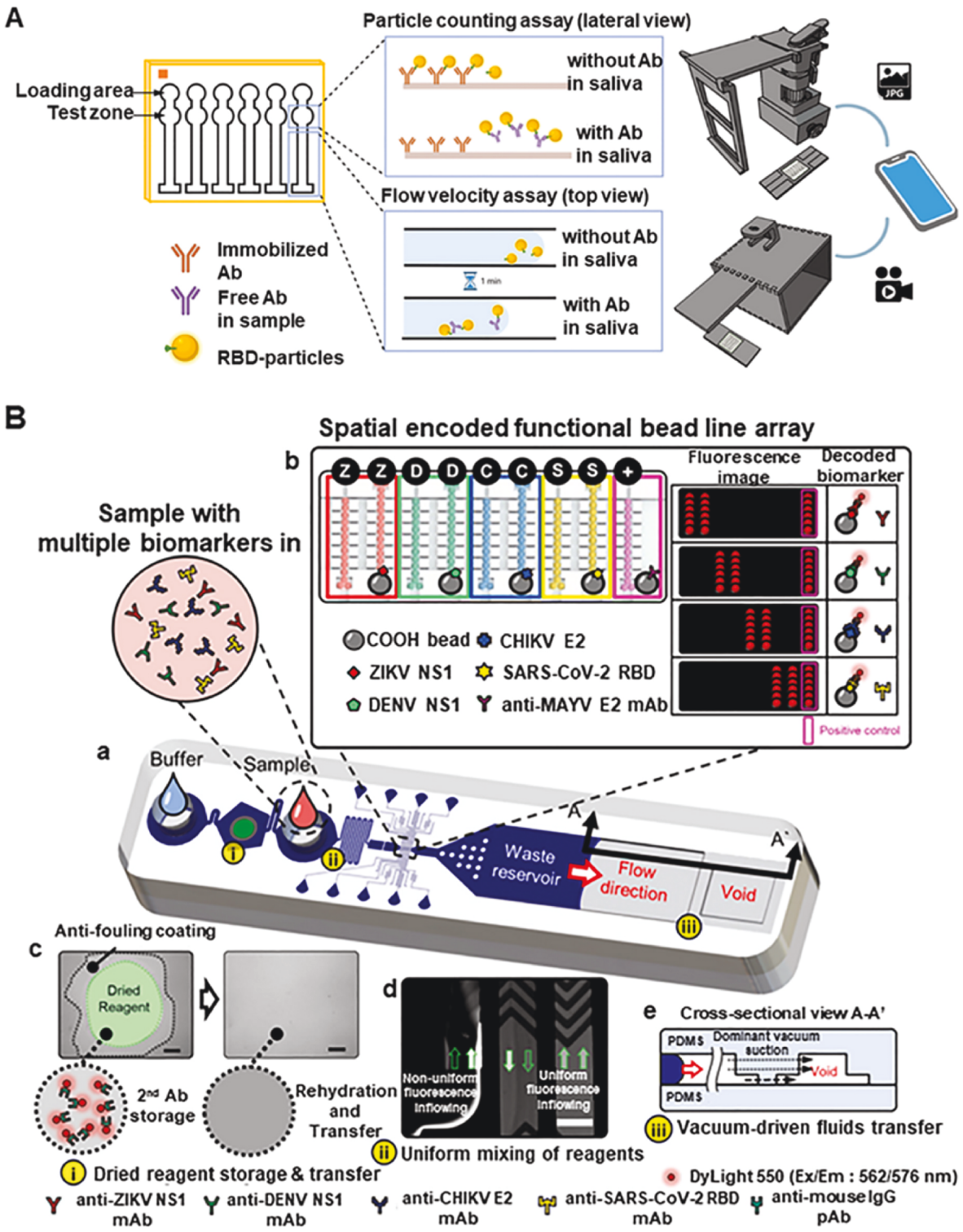

Fig. 4. Fluorescent microfluidic immunoassays for SARS-CoV-2. (A) Scheme of the paper-based fluorescent competitive microfluidic immunoassay for *anti*-SARS-CoV-2 IgG based on particle counting and measurement of flow velocity using a smartphone. Adapted with permission from Ref. [119]. Copyright 2023 Elsevier. (B) Scheme of the single snapshot fluorescent microfluidic device for multiplexed immunoassay of anti-arbovirus and SARS-CoV-2 antibodies using dense test lines and engineered beads. (a) Layout of the snapshot microfluidic device. (b) Fluorescent immunoassay principle using individually engineered high-density test lines in the reaction zone. (c) Protocol for storage and transfer of reagents in the device. (d) Photographic illustration of mixing of reagents in the device. (e) Illustration of vacuum-driven fluid transfer in the device. Adapted with permission from Ref. [120]. Copyright 2021 Elsevier.

the immuno-complexes in the paper channels using a smartphone. The assay showed LODs of 1.0–5.0 ng/mL in both 10 % and 1 % saliva in the detection. The same group presented another paper-based fluorescent microfluidic chip for testing airborne inactivated SARS-CoV-2 [121]. After air sampling (i.e., spraying) on a four-channel paper chip, fluorescent PS particle-labeled *anti*-SARS-CoV-2 antibodies were loaded into the chip. Based on a similar mechanism, a smartphone-based fluorescent microscope was designed to read the detection signals. This was a direct

and instrument-free approach to test SARS-CoV-2 in bioaerosols. The total runtime from capture to detection was less than 30 min.

Polymer-based and relevant hybrid microfluidic devices are also of particular interest for developing fluorescent immunoassays for SARS-CoV-2, due to the excellent transparency and low background inference of the substrates. Some conventional fluorescent immunoassays can be flexibly integrated into these microfluidic chips [75]. For instance, Fang et al. developed a portable polycarbonate-based lateral chromatography immunoassay for SARS-CoV-2 N protein and IgG in pharyngeal swab samples and serum, respectively, using fluorescent carboxylate-modified microparticles (FMSs) as the probe [122]. Due to the minor interaction area between FMSs and the chip surface, the FMS-labeled capture antibody detached from the chip after binding with the targets in the capture zone. The immuno-complexes then flowed into microfluidic channels under the capillary effect and reacted with the immobilized detection antibody in the test zone. N protein and IgG were detected at LODs of 0.85 ng/mL and 5.80 ng/mL with broad linear ranges of 0.15–150 ng/mL and 1.0–100 ng/mL, respectively. Furthermore, the chip showed a satisfactory stability in the testing results during the storage for varying days within one week. Garcia-Cordero et al. reported a multiplexed fluorescent microfluidic immunoassay for serological *anti*-SARS-CoV-2 antibodies using a mechanically induced trapping of molecular interactions (MITOMI) technique [63]. Two PMMA sheets containing manifolds were adhered to a glass substrate to seal the microfluidic environment. Based on the pressure-driven mechanism, the MITOMI technique was integrated to control the fluid flow in microchannels, through which phycoerythrin (PE)-conjugated secondary antibodies interacted with the targets. Excessive reagents that did not participant in the reaction were also removed *via* the technique. The device exhibited a sensitivity of 95 % and a specificity of 91 % in the detection. Kim et al. developed a single snapshot fluorescent microfluidic device for multiplexed immunoassay of anti-arbovirus and SARS-CoV-2 antibodies using dense test lines in combination with engineered beads [120]. As illustrated in Fig. 4B, antigen-conjugated carboxylate PS beads were individually engineered (or positioned) as nine high-density test lines in central microchannels in the reaction zone of the PDMS chip. In the presence of target antibodies, the fluorescence in the test lines was activated as a result of the corresponding immuno-recognition using DyLight 550 to label the detection antibodies (i.e., secondary antibodies). A portable fluorescence reader was employed to record snapshots of the bead lines. As such, four types of antibodies to both arbovirus and SARS-CoV-2 were detected simultaneously within 30 min.

3.2.3. Chemiluminescence detection

Chemiluminescence (CL) is a popular biosensing principle that works on the measurement of emitted luminescence by chemical reactions [123–125]. It is based on the transition of electrons from substances in the luminescence mechanism. In comparison with fluorescence, CL has lower background signals and higher sensitivity without the need of external light sources [126,127]. The implementation of signal readout in this principle is similar to that of fluorescence in POCT [128]. In combination with other luminescent substrates, such as luminol and trichloropyridine ruthenium (Ru $(bpy)_3^{2+}$), nanomaterials are widely used as catalysts, luminescent materials or fluorescence acceptors to improve the analytical performance in immunoassays of SARS-CoV-2 [129].

CL has been integrated into microfluidic devices for the immunoassay of SARS-CoV-2. For example, Seidel et al. presented a CL-based microarray immunoassay for serological IgG against SARS-CoV-2 [130]. The microarray chip was fabricated by polycarbonate and contained an interesting flow cell design. This design needed low volumes of samples and enabled uniform reagent distribution in an automated way. After chemical modification of the microarrays to prevent non-specific binding, the differentiation between positive and negative samples was well achieved even under high interfering conditions. Using luminol as the luminescent probe and HRP to label the detection antibodies, the immunoassay allowed for 100 % sensitivity and good specificity. Yan et al. reported a CL-based LFIA for SARS-CoV-2 recombinant S protein using Co–Fe@hemin-peroxidase nanozymes as the probe, as shown in Fig. 5 [18]. The nanozymes were synthesized by a hydrothermal method and were used to label the detection antibody to establish the sandwich-type immunoassay system in the LFIA strip. The nanozymes possessed strong peroxidase-like activity in catalyzing luminol, through which the CL detection signals were amplified. The test time was reduced to 16 min. By employing a smartphone camera to record the CL images for signal readout, recombinant S protein was determined at the LOD of 0.1 ng/mL with a linear range of 0.2–100 ng/mL.

3.2.4. Surface-enhanced Raman scattering detection

Based on the Raman scattering characters of biomolecules on nanostructured materials, surface-enhanced Raman scattering (SERS) has drawn considerable interest for developing microfluidic immunoassays [131,132]. Due to its high sensitivity and specificity, SERS is capable of fingerprinting the structures of analytes at trace contents. Metal nanomaterials such as Au NPs and Ag NPs are popular nanotags in SERS-based immunoassays. By plasmon-mediated enhancement of electrical fields, these nanomaterials can be functionalized or coupled to Raman reporters to amplify the SERS signals [133]. Interestingly, microfluidic devices are compatible with portable Raman spectrometers to achieve simple signal outcome, making them more suitable for POCT [134,135].

Taking advantages of LFIAs in POCT, SERS-based LFIAs have been widely reported for the immunoassay of SARS-CoV-2 [138]. Wang et al. developed a SERS-based LFIA for *anti*-SARS-CoV-2 IgG and IgM in serum using 5,5-dithiobis-(2-nitrobenzoic acid) (DTNB)-loaded SiO_2@Ag NPs as the SERS tags [136]. As shown in Fig. 6A, two layers of DTNB were separately adsorbed in SiO_2@Ag core-shell nanocomposites using polyethyleneimine (PEI), Au seeds and Ag shells as the intermediate layers, followed by the conjugation with S protein. In the LFIA strip, the tags showed sensitive SERS signals with high monodispersity and satisfactory stability after their immuno-capture in test lines. By employing a portable Raman spectrometer for signal readout, the assay showed 100 % accuracy and specificity in testing 68 clinical serum samples. The LOD was 800 times lower than that of the conventional Au NPs-based LFIA. Zeng et al. synthesized ultrathin Au-coated Ag NPs with the embedding of 4-mercaptobenzoic acid (MBA) (Ag^{MBA}@Au), and used the nanocomposites as a colorimetric/SERS dual-mode probe in a LFIA for *anti*-SARS-CoV-2 IgG [139]. In the nanocomposites, strong electromagnetic field was generated by enhanced plasma ascribed to the gap between Ag nanocores and Au shells. The SERS signals were further amplified by embedding MBA. Using the nanocomposites to label the detection antibody, IgG was determined at a LOD of 0.22 pg/mL in buffer solutions and 0.52 pg/mL in serum, respectively. A satisfactory accuracy of the method was demonstrated in testing 107 clinical serum samples. Choo et al. constructed a SERS-based LFIA for SARS-CoV-2 N protein in nasopharyngeal swab samples using a portable SERS-LFIA reader [84]. In this work, malachite green isothiocyanates (MGITCs) acted as the Raman reporter with the aid of Au NPs to amplify the SERS signals. Employing a mapping technique and an averaging process to measure the signal intensity, the SERS-LFIA reader exhibited good reproducibility. N protein was tested with a LOD of 3.53 PFU/mL. The method showed higher sensitivity in testing clinical samples in comparison with the commercial LFIA. Huang et al. developed a SERS-based LFIA for simultaneous detection of *anti*-SARS-CoV-2 IgG and IgM in serum using gap-enhanced Raman nanotags [140]. 4-Nitrobenzenethiol (4-NBT) as the Raman reporter was first modified on surfaces of Au nanocores and then coated with Au nanoshells to prepare the gap-enhanced nanotags. Using the nanotags to label the detection antibodies in the strip, it was demonstrated that the sensitivity was significantly improved. IgG and IgM were determined at LODs of 1.0 ng/mL and 0.1 ng/mL, respectively.

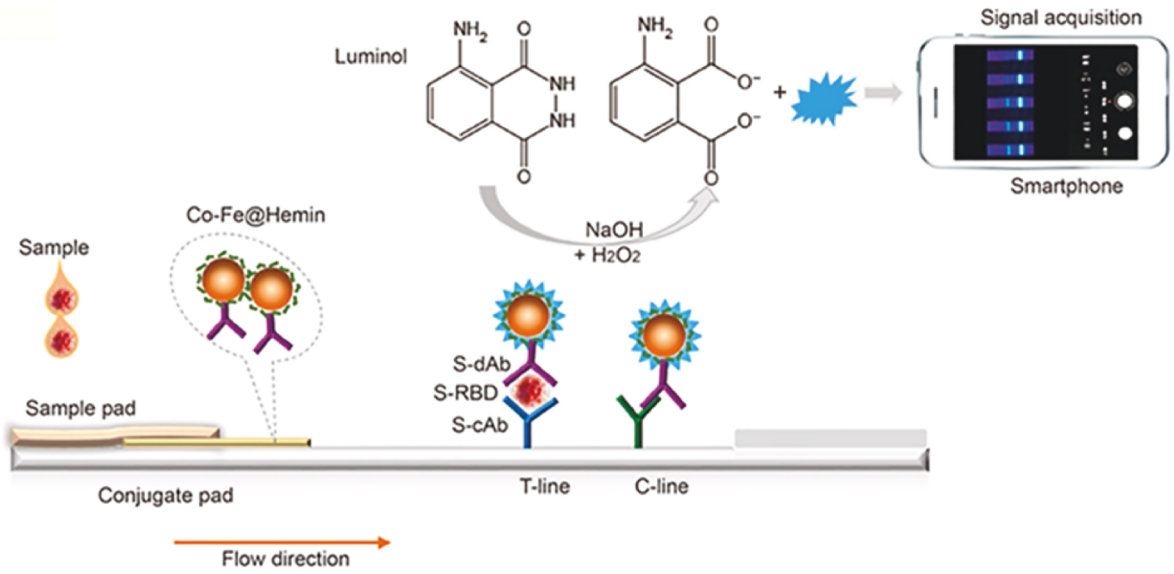

Fig. 5. Scheme of layout and working principle of the CL-based LFIA for SARS-CoV-2 recombinant S protein using Co–Fe@hemin-peroxidase nanozymes as the probe. Adapted with permission from Ref. [18]. Copyright 2020 Elsevier.

SERS can be integrated into polymer-based microfluidic devices using these nanotags for the immunoassay of SARS-CoV-2. Choo et al. reported a PDMS-based microdroplet sensor for SARS-CoV-2 N protein in nasopharyngeal swab samples using hollow gold nanospheres as the SERS nanotags [137]. As shown in Fig. 6B, oil, nanotag-labeled detection antibodies, magnetic bead-conjugated capture antibodies and pathogen lysates containing N protein were simultaneously injected into the chip to generate droplets containing the sandwich-type immuno--complexes. The droplets were then splintered with the aid of an embedded magnet to isolate the free nanotags from the immuno-complexes. The SERS signals of the nanotags in supernatants were monitored with a Raman microscope. Due to the ensemble average effect, the device exhibited high sensitivity and good reproducibility with a LOD of 0.22 PFU/mL for N protein. Shen et al. developed a glass/PDMS-based label-free opto-microfluidic immunoassay for *anti*--SARS-CoV-2 S protein antibodies in serum [141]. In the device, the glass substrate was modified with a layer of gold nanospikes *via* electrodeposition, which were then conjugated with the capture antigen. Upon the specific antigen-antibody binding on the nanospikes, local refractive index changes were generated to implement the detection. The authors clarified that the device was suitable for detecting complicated samples, as the short decay length of the electromagnetic field could reduce the interference. *Anti*-SARS-CoV-2 S protein antibodies were tested at a LOD of 0.5 pM in plasma.

3.2.5. *Electrochemical detection*

Electrochemistry has been the subject of extensive research for developing quantitative microfluidic immunoassays for SARS-CoV-2, due to its high sensitivity, good specificity and ease of integration into portable or wearable devices [142,143]. For instance, the fabrication of the typical three-electrode arrays on paper and polymer substrates can be easily achieved by techniques such as screen printing and electronic sputtering [144]. Based on the electrochemical properties (e.g., electrocatalytic activity and conductivity), nanomaterials especially for carbon-based ones (e.g., GO and carbon nanotubes) are widely employed to modify the electrodes or serve as electroactive probes to improve the analytical performance [145,146]. Furthermore, electrochemical circuits can be coupled to or miniaturized into microfluidic devices to allow for the output of detection signals *via* portable electronics like cellphones, making them very suitable for real-time and on-site detection [147]. These features provide electrochemical microfluidic immunoassays substantial potential in POCT of SARS-CoV-2.

μPADs and relevant hybrid devices are excellent candidates for developing electrochemical microfluidic immunoassays for SARS-CoV-2, due to their aforementioned advantages. Chaiyo et al. developed a paper-based label-free electrochemical microfluidic immunoassay for *anti*-SARS-CoV-2 IgG and IgM in real sera samples [61]. As shown in Fig. 7A, the device had an origami structure with the printing of electrodes in different layers. To improve the stability and reproducibility of the device, a reversed electrode architecture was fabricated by embedding GO in porous paper networks of the working zones *via* hydrogen bonding and physical adsorption. Based on the effect of specific immuno-binding on the redox conversion of $[Fe(CN)_6]^{3-/4-}$ on electrode surfaces, the device showed sensitive SWV signals in response to the targets. Using a cellphone for signal output, IgG and IgM were detected at LODs of 0.96 ng/mL and 0.14 ng/mL, respectively, with a broad linear range of 1–1000 ng/mL for both. Henry et al. reported a sandwich-type electrochemical microfluidic immunoassay for *anti*-SARS-CoV-2 N protein IgG in whole blood [148]. Interestingly, a blood-filtration membrane was integrated into the device for on-board plasma extraction. In the assay system, HRP-labeled secondary antibody worked as the detection antibody to catalyze the generation of $_{ox}$TMB as an electroactive probe. Using in-flow chronoamperometry, the device could detect *anti*-N protein IgG at a LOD of 5.0 ng/mL, more sensitive than that of commercial ELISA kits (8.0 ng/mL).

Electrochemistry is also compatible with polymer-based microfluidic devices for the immunoassay of SARS-CoV-2, since the electrode arrays can be easily fabricated on such substrates even in large scale. Lillehoj et al. fabricated a PET/PMMA-based electrochemical microfluidic immunoassay for SARS-CoV-2 N protein in serum using dually-labeled magnetic nanobeads (DMBs) [72]. As illustrated in Fig. 7B–a PET/PMMA cartridge engraved with microchannels and a reaction chamber were stacked on a screen-printed gold electrode (SPGE) sensor to fabricate the device. Magnetic beads were labeled with both the detection antibody and HRP to prepare the DMBs that were immuno-captured on surfaces of SPGEs. With the aid of an external magnet, both the immuno-magnetic enrichment and amplification of the amperometric detection signal were achieved utilizing TMB as the substrate. The LODs of N protein in serum and in 5-fold diluted serum were as low as 50 pg/mL and 10 pg/mL, respectively, which correspondingly elevated to 230 pg/mL and 100 pg/mL when coupled with a

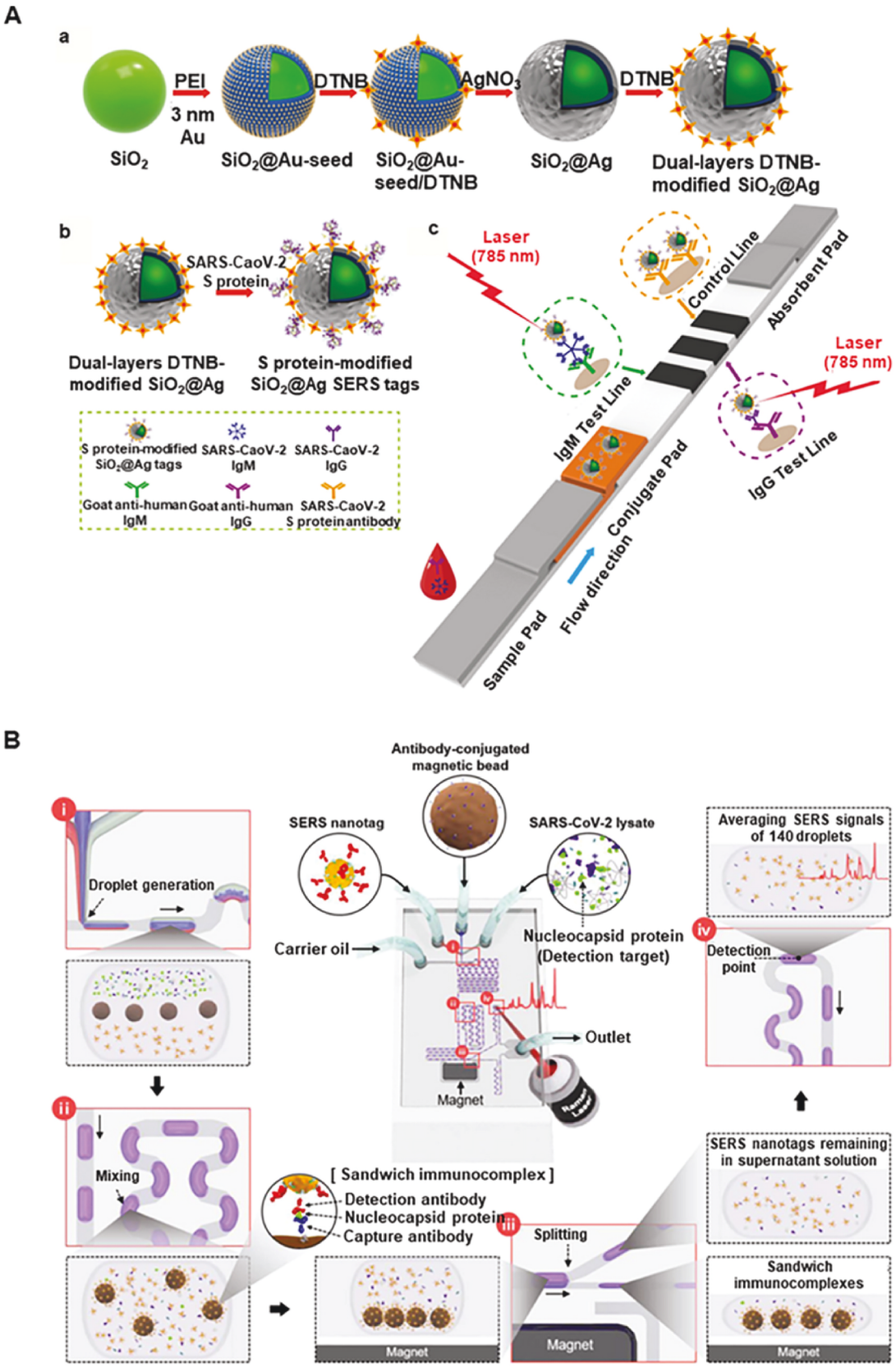

Fig. 6. Microfluidic immunoassays integrated with SERS for SARS-CoV-2 detection. (A) Scheme of the SERS-based LFIA for *anti*-SARS-CoV-2 IgG and IgM using DTNB-loaded SiO_2@Ag NPs as the SERS tags. (a) Preparation of DTNB-loaded SiO_2@Ag nanotags. (b) Conjugation of SARS-CoV-2 S protein with the nanotags. (c) Working principle of the SERS-based LFIA. Adapted with permission from Ref. [136]. Copyright 2020 Elsevier. (B) Scheme of layout and working principle of the microdroplet chip for SERS-based immunoassay of SARS-CoV-2 N protein using hollow gold nanotags with the aid of magnetic separation. Adapted with permission from Ref. [137]. Copyright 2022 Elsevier. (For interpretation of the references to colour in this figure legend, the reader is referred to the Web version of this article.)

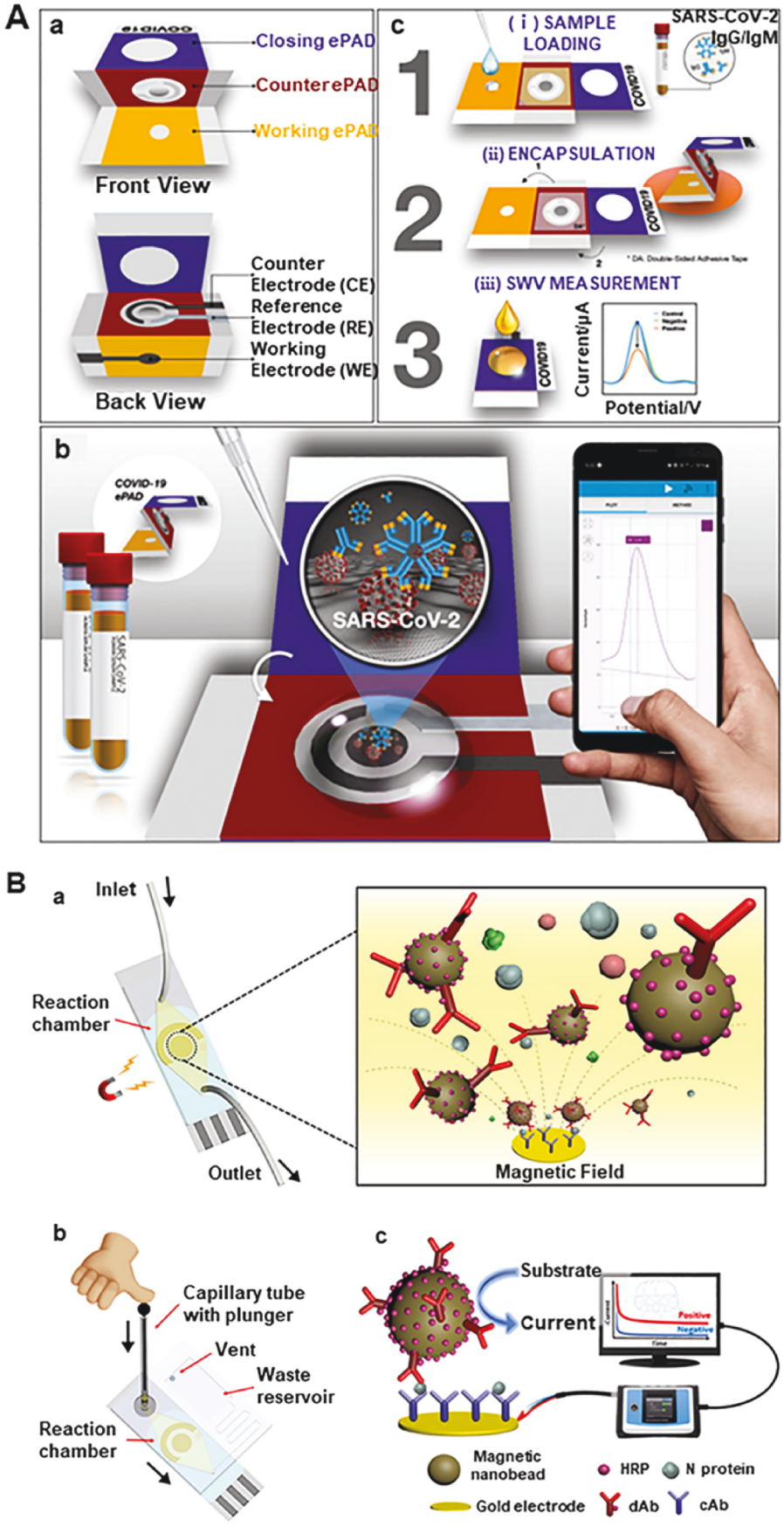

(caption on next page)

Fig. 7. Electrochemical microfluidic immunoassays for SARS-CoV-2. (A) Scheme of the paper-based label-free electrochemical microfluidic immunoassay for *anti*-SARS-CoV-2 IgG and IgM. (a) Layout of the microfluidic device. (b) Label-free electrochemical immunoassay principle using a smartphone for signal readout and (c) detection procedure. Adapted with permission from Ref. [61]. Copyright 2020 Elsevier. (B) Scheme of the PET/PMMA-based electrochemical microfluidic immunoassay for SARS-CoV-2 N protein using DMBs. (a) Illustrations of microfluidic chip using DMBs for immuno-magnetic enrichment. (b) Layout of the device and detection procedure. (c) Electrochemical immunoassay principle and the experimental setup. Adapted with permission from Ref. [72]. Copyright 2021 American Chemical Society.

smartphone for signal output. Sanati-Nezhad et al. reported a PMMA-based self-powered electrochemical microfluidic immunoassay for SARS-CoV-2 N protein in plasma [64]. With the aid of the self-powered microfluidic platform, the whole immunoassay procedure including the sequential delivery of samples and reagents was automated without the need of additional instruments. $[Fe(CN)_6]^{3-/4-}$ was used as the redox probe on screen-printed electrodes (SPEs) employing the electrochemical impedance spectroscopy for the detection. N protein was differentiated in a range of 10–1000 pg/mL with a LOD of 3.1 pg/mL. Additionally, Mahshid et al. reported a multiplexed fluidic device (NFluidEX) for the immunoassay of SARS-CoV-2 S protein and *anti*-RBD IgG and IgM in saliva and blood, respectively [149]. In the device, they integrated gold nano/micro islands (NMIs) sensors with a biomimetic receptor using molecularly imprinted polymers. The analytical data were acquired and processed on a smartphone using multiplexed impedimetric readout. It was proved that the large surface area of gold NMIs enhanced the localized electrical field confinement and amplified the electrochemical signals. S protein and *anti*-RBD antibodies were determined at LODs of 5.89 pg/mL and 3.13 pg/mL, respectively. Shen et al. developed a rapid and high-throughput microfluidic immunoassay for *anti*-SARS-CoV-2 N and S protein IgG in serum using a polyester/resin chip [150]. An electrodeposition method was used to grow gold nanoflowers on carbon black-modified SPEs, providing a large surface area to enhance the analytical performance. The immuno-captured alkaline phosphatase hydrolyzed 1-napthtyl phosphate into naphthol that was further oxidized to release electrons. Using differential pulse voltammetry (DPV), *anti*-N and S protein IgG were quantitatively detected at LODs of 28 ng/mL and 15 ng/mL, respectively.

The 3D printing technique was also widely used in fabricating electrode arrays in developing electrochemical microfluidic immunoassays. For instance, Ingber et al. constructed a 3D-printed electrochemical microfluidic immunoassay for *anti*-SARS-CoV-2 antibodies in plasma [151]. 3D-printed gold electrode arrays were coated with antifouling layers consisting of bovine serum albumin (BSA) and reduced graphene (rGOx) that were crosslinked with glutaraldehyde (GA) (BSA/rGOx/GA). HRP was utilized to label the detection antibodies to establish the immunoassay system. Using cyclic voltammetry (CV) and TMB as the substrate, the lab-on-a-chip platform exhibited superior electrochemical conductivity and low non-specific binding. Significantly, the multiplexed detection of diverse antibodies (i.e., IgG, IgM or IgA) against relevant antigens was achieved in clinical plasma samples, and the results showed good consistency with that of conventional ELISAs. Panat et al. fabricated a glass/PDMS-based electrochemical microfluidic immunoassay for detecting *anti*-SARS-CoV-2 S1 protein and RBD antibodies using nanoprinted 3D electrodes [152]. The electrode arrays were fabricated by a 3D nanoprinting approach, followed by coating with nanoflakes of reduced GO (rGO) for immobilization of capture antigens. By a low-pH chemical routine to undermine the binding between antigens and antibodies, the device can be reused. *Anti*-S1 protein and RBD antibodies were detected at LODs of 2.8×10^{-15} and 16.9×10^{-15} M, respectively.

3.2.6. *Photothermal biosensing and distance-based detection*

In recent years, some newly emerging biosensing principles such as quantitative photothermal biosensing using a thermometer pioneered by the Li group have been applied to microfluidic devices for POCT [21,28,92,94,95] [93,100]. Based on the new exploitation of chemical and physical principles, advances especially in signal transduction and output in microfluidic devices were reported by researchers worldwide. For instance, the photothermal effect has been applied in microfluidic chips for simple, precise and remotely tunable pumping of reagents by using portable laser pointers [27,153,154]. Very recently, the photothermal biosensing is integrated into microfluidic chips to enable the quantitative bar-chart visualization of immunoassay signals [22,154–156].

Photothermal effect is a photo-physical principle that the light energy is converted into heat energy by photothermal agents thorough different mechanisms [40,93,158–161]. Accordingly, the photothermal biosensing utilizes photothermal effect to convert the molecule-recognition events from traditional ones into heat signals [155]. Handheld temperature readers like thermometers and thermal cameras can be used for quantitative signal readout [40,159]. Very recently, the photothermal biosensing has been applied for microfluidic immunoassay of SARS-CoV-2. Zhang et al. developed a photothermal LFIA for *anti*-SARS-CoV-2 S protein IgG in serum using rhenium diselenide ($ReSe_2$) nanosheets as the photothermal probe [34]. As shown in Fig. 8A, $ReSe_2$ nanosheets with high surface area and photothermal efficiency were prepared by a liquid exfoliation approach, followed by conjugation with S protein to construct the immunoassay system in the LFIA strip. A portable 808-nm laser pointer was employed to irradiate the test and control lines in the strip. Subsequently, a smartphone-based thermal imager was used for quantitative readout of the temperature signals. The LFIA detected *anti*-SARS-CoV-2 S protein IgG at a LOD of 0.86 ng/mL and could discriminate varying concentrations in a range from 1.0 ng/mL to 10 μg/mL. Bischof et al. developed a LIFA for SARS-CoV-2 RBD antigen (S protein) in nasopharyngeal wash using a thermal contrast amplification (TCA) strategy [162]. Gold nanospheres (GNSs) were labeled with the detection antibody and worked as the photothermal probe in the immunoassay system. Owing to their large absorption cross sections and massive specific binding sites, GNSs exhibited significantly amplified thermal signals upon laser irradiation, displaying high sensitivity at fM-aM levels. RBD antigen was determined at LODs of 0.45 aM and 3.6 aM in buffers and human nasopharyngeal wash samples, respectively. Tabatabaei et al. presented a thermo-photonic device for the immunoassay of *anti*-SARS-CoV-2 RBD IgG by integrating LFIA with a portable signal reader [32]. In the indirect LFIA, Au NPs acted as a colorimetric/photothermal dual-model probe in the test zones. Both the LFIA strip and a smartphone-based infrared camera were assembled in a portable device with the aids of lens and control electronics. *Anti*-RBD IgG was tested at a LOD of 0.1 μg/mL, and the coefficient of variation was 1.89 % in repeated testing of 40 samples.

In addition, the distance-based detection is of particular interest for developing microfluidic immunoassays, since the distance signals can be directly and quantitatively monitored without the need of specific instruments [21,28,94,95,163]. In distance-based detection in microfluidic devices, working principles including gas-based volumetric pumping, capillary effect in paper substrates, magnetic separation, and photothermal effect-based bar-chart chips [94,95] are mostly reported, some of which have been applied for microfluidic immunoassay of SARS-CoV-2 [164,165]. Liu et al. reported a hand-powered centrifugal micropipette tip for the immunoassay of SARS-CoV-2 N protein in nasal swab samples [166]. In the pipette tips, the specific binding between N protein and red latex nanobead-labeled antibody led to the aggregation of nanobeads. Upon the hand-powered centrifugation of the tips, the

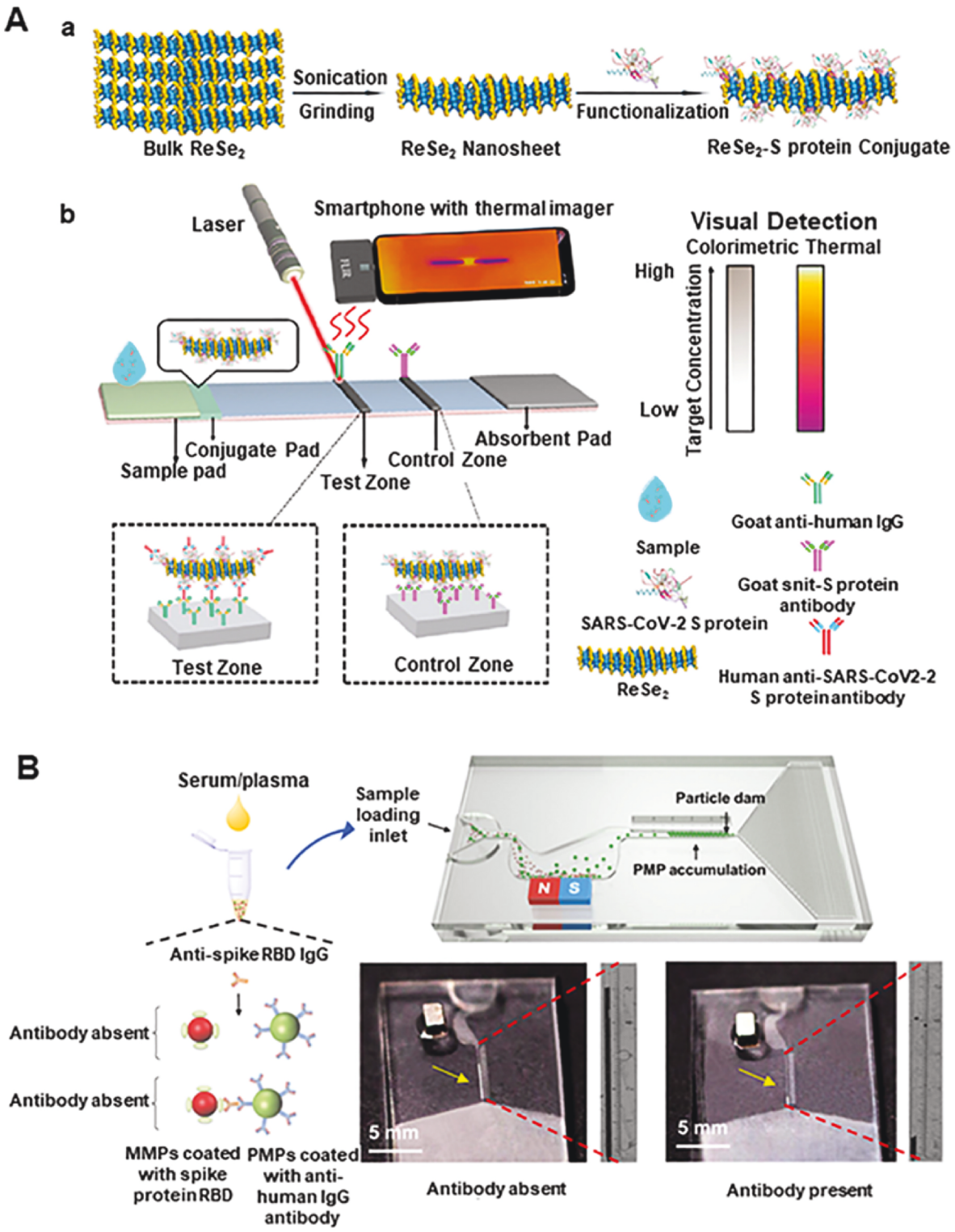

Fig. 8. Microfluidic immunoassays for SARS-CoV-2 based on photothermal biosensing and distance-based detection. (A) Scheme of the photothermal LFIA for *anti*-SARS-CoV-2 S protein IgG using $ReSe_2$ nanosheets as the photothermal probe. (a) Preparation of $ReSe_2$ nanosheets. (b) Photothermal immunoassay principle of the LFIA using a smartphone-based thermal imager for signal readout. Adapted with permission from Ref. [34]. Copyright 2023 American Chemical Society. (B) Scheme of layout and working principle of the microfluidic immunoassay chip for *anti*-SARS-CoV-2 S protein IgG using a particle dam design for distance-based signal readout with the aid of magnetic separation. Adapted with permission from Ref. [157]. Copyright 2022 American Association for the Advancement of Science.

aggregated red immuno-complexes moved downward to the bottom, whereas free nanobeads remained in upper solutions. By reading the gray value of the cumulative area in the tips as the assay signal, N protein was tested at the LOD of 1.0 ng/mL. Yoon et al. established a paper-based microfluidic immunoassay for SARS-CoV-2 N protein in saliva samples by analyzing the capillary flow velocity profiles in paper channels [167]. The formation of immuno-complexes between PS article-labeled antibody and N protein altered the surface tension along

with changing capillary flow velocity in the paper channels. Employing a smartphone to record and analyze the flow velocity profiles, N protein was tested at LODs of 1.0 fg/mL in saliva and 10 fg/mL in simulated saline gargle samples, respectively. The accuracy of the method was 89 % in testing 18 clinical saline gargle samples. Chen et al. developed a simple method for microfluidic immunoassay of *anti*-SARS-CoV-2 S protein IgG using magnetic separation in combination with an interesting particle dam design for distance-based signal readout [157]. As shown in Fig. 8B, the immuno-reaction was first performed in a common centrifuge tube using immuno-labeled magnetic microparticles (MMPs) and polystyrene microparticles (PMPs). In the presence of target IgG, immuno-complexes were formed and then injected into the chip. Upon the intermediate blocking of the magnetic complexes using a magnet, the accumulation amounts of free PMPs in the downward dams decreased with the display of shortened visual distance. The target was tested at LODs of 13.3 ng/mL and 57.8 ng/mL in a sensitive mode and a rapid mode, respectively. More impressive work from these emerging detection principles are expected in the future.

4. Conclusions, challenges and perspectives

The POCT of SARS-CoV-2 antigens and antibodies plays a significant role in preventing the spread of the disease in the recent COVID-19 pandemic and also provides insights on developing new detection technologies for defensing against similar pandemics in the future. This article reviews recent advances in microfluidic immunoassays for POCT of SARS-CoV-2 antigens and antibodies. Various biosensing principles, such as colorimetry, electrochemistry, fluorescence, surface-enhanced Raman scattering and photothermal biosensing, have been integrated into diverse types of microfluidic devices for qualitative, semi-quantitative or quantitative immunoassays of SARS-CoV-2. We have summarized key analytical parameters of representative works in Table 2. There is no doubt that research efforts and advancements are of great potential for POCT of SARS-CoV-2 especially in resource-limited settings.

Despite these advances, it should be noted that multiple challenges are still encountered in this field especially from the view of practical utility of these microfluidic immunoassays. Although the LFIA is currently a major POCT tool for SARS-CoV-2 in practical usage, its sensitivity is generally lower in comparison with conventional ELISAs and NAATs. As a result, false-negative results from the LFIA are very common. At present, most traditional LFIAs and colorimetric methods are more suitable for qualitative detection but inconvenient for quantitative tests in some special analytical tasks, such as the immunity monitoring in serological investigations. As to the fluorescence, SERS, chemiluminescence and electrochemistry methods, quantitative detection is competent and the sensitivity is higher, but most methods often require sophisticated instruments (e.g., spectrometers and working stations) and skilled personnel. More efforts are still needed to miniaturize these analytical instruments and simplify the operation while reducing the price to an affordable level, though bar-chart chip and other distance-based detection hold potential for a different solution. In photothermal biosensing, the immunoassay procedures are often tedious and it is highly desirable to integrate lasers and temperature readers into a portable device. Regarding the operation of some microfluidic devices, the requirement of external accessories like pipettes or pumps for reagent handling can be another barrier for POCT. These limitations compromise their potential for practical applications in POCT to some extent. Additionally, as a competitor to emerging POC-based commercial qPCR devices with rapidness and high sensitivity such as Xpert Xpress SARS-CoV-2, more improvements are needed to make immunoassays more robust, convenient, sensitive, cost-effective, and higher-throughput.

Therefore, more research efforts are indispensable to cope with these challenges. To improve the analytical performance (e.g., sensitivity), new strategies such as nanomaterial-modulated signal amplification [71,168–173] are expected to work with these microfluidic immunoassays especially for the LFIA. Pre-enrichment can be another strategy to improve the detection sensitivity [41]. From the aspect of biosensing principle, the development of new signal transduction principles such as multi-colorimetric immunosensors [106] to enable visual quantitative signal readout using portable and affordable analyzers (e.g., smartphones [174–176]) might be an ideal thought to avoid the usage of specific analytical instruments. Similarly, the coupling of microfluidic chips with some household healthcare devices (e.g., thermometers [92,93,100,177,178] and glucometers [179,180]) for quantitative signal readout is intriguing. From the aspect of device operation, the integration of intelligent programmable controllers with electronic micro-pumps is capable of providing automatic, accessory-free but precise handling of reagents. On the other hand, the combination of pump-free microfluidic mixers with paper-based devices is a promising strategy for POCT because of its simplicity and reliability compared to conventional microfluidics in reagent handling. For example, Henry et al. developed a pump-free microfluidic device that enabled rapid, uniform and stable mixing of reagents by integrating paper layers with plastic passive mixers for colorimetric detection of Malathion [181]. This strategy provides an efficient way to solve some limitations (e.g., uncontrollability in flow rate and non-uniform mixing of liquid reagents) of inherent capillary force-driven liquid handling in paper substrates, which show great potential for paper-based microfluidic POC immunoassays. Furthermore, we believe that the collaboration among different disciplines such as medicine, biomedical engineering, material science and artificial intelligence is vital to translate these microfluidic immunoassays from laboratories to practical POCT usage for SARS-CoV-2 detection [182].

CRediT authorship contribution statement

Cuili Li: Writing – original draft, Investigation. **Wan Zhou:** Writing – original draft, Investigation. **Angel Gutierrez Ruiz:** Writing – original draft, Investigation. **Yasaman Mohammadi:** Writing – original draft, Investigation. **Qingning Li:** Writing – original draft, Investigation. **Shuting Zhang:** Writing – original draft, Conceptualization. **XiuJun Li:** Writing – review & editing, Writing – original draft, Supervision, Project administration, Funding acquisition, Conceptualization. **Guanglei Fu:** Writing – review & editing, Writing – original draft, Supervision, Conceptualization.

Declaration of competing interest

The authors declare that they have no known competing financial interests or personal relationships that could have appeared to influence the work reported in this paper.

Data availability

No data was used for the research described in the article.

Acknowledgements

This research was fanatically supported by the Research Starting Foundation of Yantai University (2222006), U.S. NIH/NIAID (R41AI162477), U.S. NSF (IIP2122712 and CHE2216473), and the Cancer Prevention and Research Institute of Texas (CPRIT; RP210165).

References

[1] F. Wu, S. Zhao, B. Yu, Y.M. Chen, W. Wang, Z.G. Song, Y. Hu, Z.W. Tao, J.H. Tian, Y.Y. Pei, M.L. Yuan, Y.L. Zhang, F.H. Dai, Y. Liu, Q.M. Wang, J.J. Zheng, L. Xu, E. C. Holmes, Y.Z. Zhang, Nature 580 (2020) 265.
[2] M. Ciotti, M. Ciccozzi, A. Terrinoni, W.C. Jiang, C.B. Wang, S. Bernardini, Crit. Rev. Clin. Lab Sci. 57 (2020) 365.

[3] WHO COVID-19 Dashboard, 7 April 2024, World Health Organization, Geneva, 2024. https://data.who.int/dashboards/covid19/deaths?n=c.
[4] M.Y. Wang, R. Zhao, L.J. Gao, X.F. Gao, D.P. Wang, J.M. Cao, Front. Cell. Infect. Microbiol. 10 (2020) 587269.
[5] A.M. Carabelli, T.P. Peacock, L.G. Thorne, W.T. Harvey, J. Hughes, S.J. Peacock, W.S. Barclay, T.I. de Silva, G.J. Towers, D.L. Robertson, Nat. Rev. Microbiol. 21 (2023) 162.
[6] R. Liu, H. Han, F. Liu, Z. Lv, K. Wu, Y. Liu, Y. Feng, C. Zhu, Clin. Chim. Acta 505 (2020) 172.
[7] A.J. Colbert, D.H. Lee, K.N. Clayton, S.T. Wereley, J.C. Linnes, T.L. Kinzer-Ursem, Anal. Chim. Acta 1203 (2022) 339702.
[8] A.A. Zasada, E. Mosiej, M. Prygiel, M. Polak, K. Wdowiak, K. Forminska, R. Ziolkowski, K. Zukowski, K. Marchlewicz, A. Nowinski, J. Nowinska, W. Rastawicki, E. Malinowska, Biomedicines 10 (2022) 2329.
[9] J.P. Broughton, X. Deng, G. Yu, C.L. Fasching, V. Servellita, J. Singh, X. Miao, J. A. Streithorst, A. Granados, A. Sotomayor-Gonzalez, K. Zorn, A. Gopez, E. Hsu, W. Gu, S. Miller, C.Y. Pan, H. Guevara, D.A. Wadford, J.S. Chen, C.Y. Chiu, Nat. Biotechnol. 38 (2020) 870.
[10] W.J. Wiersinga, A. Rhodes, A.C. Cheng, S.J. Peacock, H.C. Prescott, JAMA 324 (2020) 782.
[11] H. Zhang, L. Cao, J. Brodsky, I. Gablech, F. Xu, Z. Li, M. Korabecna, P. Neuzil, TrAC, Trends Anal. Chem. 174 (2024) 117676.
[12] N. Shaver, A. Bennett, A. Beck, N. Vyas, G. Zitiktye, E. Lam, B. Whelan, R. O'Regan, A. Conway, B. Skidmore, D. Moher, J. Little, Eur. J. Clin. Invest. 53 (2023) e14058.
[13] A.C. Hunt, B. Vögeli, A.O. Hassan, L. Guerrero, W. Kightlinger, D.J. Yoesep, A. Krüger, M. DeWinter, M.S. Diamond, A.S. Karim, M.C. Jewett, Nat. Commun. 14 (2023) 3897.
[14] M.D.B. Ndiaye, L.T. Rasoloharimanana, S.L. Razafimahatratra, R. Ratovoson, V. Rasolofo, P. Ranaivomanana, L. Raskine, J. Hoffmann, R. Randremanana, N. Rakotosamimanana, M. Schoenhals, Heliyon 9 (2023) e17264.
[15] Z.J. Cheng, B. Li, Z. Zhan, Z. Zhao, M. Xue, P. Zheng, J. Lyu, C. Hu, J. He, R. Chen, B. Sun, Clin. Rev. Allergy Immunol. 64 (2023) 17.
[16] K. Srinivasan Rajsri, M.P. McRae, N.J. Christodoulides, I. Dapkins, G. W. Simmons, H. Matz, H. Dooley, D. Fenyö, J.T. McDevitt, Bioengineering (Basel) 10 (2023) 670.
[17] C. Wang, D. Shi, N. Wan, X. Yang, H. Liu, H. Gao, M. Zhang, Z. Bai, D. Li, E. Dai, Z. Rong, S. Wang, Analyst 146 (2021) 3908.
[18] D. Liu, C. Ju, C. Han, R. Shi, X. Chen, D. Duan, J. Yan, X. Yan, Biosens. Bioelectron. 173 (2021) 112817.
[19] S.T. Sanjay, W. Zhou, M. Dou, H. Tavakoli, L. Ma, F. Xu, X. Li, Adv. Drug Deliv. Rev. 128 (2018) 3.
[20] H. Tavakoli, W. Zhou, L. Ma, S. Perez, A. Ibarra, F. Xu, S. Zhan, X. Li, TrAC, Trends Anal. Chem. 117 (2019) 13.
[21] X. Wei, W. Zhou, S.T. Sanjay, J. Zhang, Q. Jin, F. Xu, D.C. Dominguez, X. Li, Anal. Chem. 90 (2018) 9888.
[22] W. Zhou, G. Fu, X. Li, Anal. Chem. 93 (2021) 7754.
[23] M. Dou, N. Macias, F. Shen, J.D. Bard, D.C. Domínguez, X. Li, EClinicalMedicine 8 (2019) 72.
[24] W. Zhou, M. Dou, S.S. Timilsina, F. Xu, X. Li, Lab Chip 21 (2021) 2658.
[25] K.S. Prasad, X. Cao, N. Gao, Q. Jin, S.T. Sanjay, G. Henao-Pabon, X. Li, Sensor. Actuator. B Chem. 305 (2020) 127516.
[26] M. Dou, J. Sanchez, H. Tavakoli, J.E. Gonzalez, J. Sun, J. Dien Bard, X. Li, Anal. Chim. Acta 1065 (2019) 71.
[27] G. Fu, W. Zhou, X. Li, Lab Chip 20 (2020) 2218.
[28] H. Tavakoli, S. Mohammadi, X. Li, G. Fu, X. Li, TrAC, Trends Anal. Chem. 157 (2022) 116806.
[29] J. Dong, H. Ueda, Wiley Interdiscipl. Rev. Nanomed. Nanobiotechnol. 9 (2017) e1457.
[30] H. Yuan, P. Chen, C. Wan, Y. Li, B.F. Liu, TrAC, Trends Anal. Chem. 157 (2022) 116814.
[31] S. Cavalera, B. Colitti, S. Rosati, G. Ferrara, L. Bertolotti, C. Nogarol, C. Guiotto, C. Cagnazzo, M. Denina, F. Fagioli, F. Di Nardo, M. Chiarello, C. Baggiani, L. Anfossi, Talanta 223 (2021) 121737.
[32] D. Thapa, N. Samadi, N. Tabatabaei, IEEE Sensor. J. 21 (2021) 18504.
[33] C. Wang, X. Cheng, L. Liu, X. Zhang, X. Yang, S. Zheng, Z. Rong, S. Wang, ACS Appl. Mater. Interfaces 13 (2021) 40342.
[34] W. Hao, Y. Huang, L. Wang, J. Liang, S. Yang, L. Su, X. Zhang, ACS Appl. Mater. Interfaces 15 (2023) 9665.
[35] H.M. Yoo, I.H. Kim, S. Kim, Int. J. Mol. Sci. 22 (2021) 6150.
[36] M.M. Islam, D. Koirala, Anal. Chim. Acta 1209 (2022) 339338.
[37] B.D. Kevadiya, J. Machhi, J. Herskovitz, M.D. Oleynikov, W.R. Blomberg, N. Bajwa, D. Soni, S. Das, M. Hasan, M. Patel, A.M. Senan, S. Gorantla, J. McMillan, B. Edagwa, R. Eisenberg, C.B. Gurumurthy, S.P.M. Reid, C. Punyadeera, L. Chang, H.E. Gendelman, Nat. Mater. 20 (2021) 593.
[38] Y.N. Tang, D. Jiang, X. Wang, Y. Liu, D. Wei, Chin. Chem. Lett. (2023) 108688.
[39] W. Zhou, M. Dou, S.S. Timilsina, F. Xu, X. Li, Lab Chip 21 (2021) 2658.
[40] W. Zhou, J. Sun, X. Li, Anal. Chem. 92 (2020) 14830.
[41] S.T. Sanjay, M. Li, W. Zhou, X. Li, X. Li, Microsyst. Nanoeng. 6 (2020) 28.
[42] W. Zhou, M. Feng, A. Valadez, X. Li, Anal. Chem. 92 (2020) 7045.
[43] L.E. Breshears, B.T. Nguyen, P. Akarapipad, K. Sosnowski, K. Kaarj, G. Quirk, J. L. Uhrlaub, J. Nikolich-Zugich, M. Worobey, J.Y. Yoon, PNAS Nexus. 1 (2022) pgac028.
[44] K.T.L. Trinh, H.D.K. Do, N.Y. Lee, Biosensors 13 (2023) 490.
[45] D. Wang, Y. Chen, S. Xiang, H. Hu, Y. Zhan, Y. Yu, J. Zhang, P. Wu, F.Y. Liu, T. Kai, P. Ding, Front. Cell. Infect. Microbiol. 12 (2022) 1040248.
[46] J. Budd, B.S. Miller, N.E. Weckman, D. Cherkaoui, D. Huang, A.T. Decruz, N. Fongwen, G.-R. Han, M. Broto, C.S. Estcourt, J. Gibbs, D. Pillay, P. Sonnenberg, R. Meurant, M.R. Thomas, N. Keegan, M.M. Stevens, E. Nastouli, E.J. Topol, A. M. Johnson, M. Shahmanesh, A. Ozcan, J.J. Collins, M. Fernandez Suarez, B. Rodriguez, R.W. Peeling, R.A. McKendry, Nat. Rev. Bioeng. 1 (2023) 13.
[47] A.S. Lee, S.M. Kim, K.R. Kim, C. Park, D.-G. Lee, H.J. Cha, H.R. Heo, C.S. Kim, Sensor. Actuator. B Chem. 379 (2023) 133245.
[48] C. Li, Z. Zou, H. Liu, Y. Jin, G. Li, C. Yuan, Z. Xiao, M. Jin, Talanta 225 (2021) 122064.
[49] W.W. Hsiao, T.N. Le, D.M. Pham, H.H. Ko, H.C. Chang, C.C. Lee, N. Sharma, C. K. Lee, W.H. Chiang, Biosensors 11 (2021) 295.
[50] L. Spicuzza, D. Campagna, C. Di Maria, E. Sciacca, S. Mancuso, C. Vancheri, G. Sambataro, AIMS Microbiol. 9 (2023) 375.
[51] W. He, M. Wang, P. Cheng, Y. Liu, M. You, TrAC, Trends Anal. Chem. 173 (2024) 117641.
[52] H. Tavakoli, E. Hirth, M. Luo, S. Sharma Timilsina, M. Dou, D.C. Dominguez, X. Li, Lab Chip 22 (2022) 4693.
[53] A.W. Martinez, S.T. Phillips, M.J. Butte, G.M. Whitesides, Angew. Chem., Int. Ed. Engl. 46 (2007) 1318.
[54] E. Noviana, T. Ozer, C.S. Carrell, J.S. Link, C. McMahon, I. Jang, C.S. Henry, Chem. Rev. 121 (2021) 11835.
[55] A. Bandopadhyay Anushka, P.K. Das, Eur. Phys. J. Spec. Top. 232 (2023) 781.
[56] R. Antiochia, Biosensors 11 (2021) 110.
[57] A.K. Kaushik, J.S. Dhau, H. Gohel, Y.K. Mishra, B. Kateb, N.Y. Kim, D. Y. Goswami, ACS Appl. Bio Mater. 3 (2020) 7306.
[58] H.A. Silva-Neto, I.V.S. Arantes, A.L. Ferreira, G.H.M. do Nascimento, G.N. Meloni, W.R. de Araujo, T.R.L.C. Paixão, W.K.T. Coltro, TrAC, Trends Anal. Chem. 158 (2023) 116893.
[59] S. Nishat, A.T. Jafry, A.W. Martinez, F.R. Awan, Sensor Actuator, Biol. Chem. 336 (2021) 129681.
[60] X.J. Li, C.Y. Yang, P.C.H. Li, Multidisciplinary Microfluidic and Nanofluidic Lab-On-A-Chip: Principles and Applications, 1 ed., Elsevier, 2021.
[61] A. Yakoh, U. Pimpitak, S. Rengpipat, N. Hirankarn, O. Chailapakul, S. Chaiyo, Biosens. Bioelectron. 176 (2021) 112912.
[62] F. Gong, H.X. Wei, J. Qi, H. Ma, L. Liu, J. Weng, X. Zheng, Q. Li, D. Zhao, H. Fang, L. Liu, H. He, C. Ma, J. Han, A. Sun, B. Wang, T. Jin, B. Li, B. Li, ACS Sens. 6 (2021) 2709.
[63] R. Rodriguez-Moncayo, D.F. Cedillo-Alcantar, P.E. Guevara-Pantoja, O.G. Chavez-Pineda, J.A. Hernandez-Ortiz, J.U. Amador-Hernandez, G. Rojas-Velasco, F. Sanchez-Munoz, D. Manzur-Sandoval, L.D. Patino-Lopez, D.A. May-Arrioja, R. Posadas-Sanchez, G. Vargas-Alarcon, J.L. Garcia-Cordero, Lab Chip 21 (2021) 93.
[64] F. Haghayegh, R. Salahandish, A. Zare, M. Khalghollah, A. Sanati-Nezhad, Lab Chip 22 (2021) 108.
[65] S. Xu, Y. Liu, Y. Yang, K. Zhang, W. Liang, Z. Xu, Y. Wu, J. Luo, C. Zhuang, X. Cai, Micromachines 14 (2023) 709.
[66] T.C. Cameron, A. Randhawa, S.M. Grist, T. Bennet, J. Hua, L.G. Alde, T. M. Caffrey, C.L. Wellington, K.C. Cheung, Micromachines 13 (2022) 1573.
[67] H. Chen, S. Feng, W. Zhou, Z. Li, M. Richard-Greenblatt, P. Wang, ACS Meas. Sci. Au 2 (2022) 414.
[68] X.J. Li, Y. Zhou, Microfluidic Devices for Biomedical Applications, 2 ed., Elsevier, 2021.
[69] H. Chen, Z. Li, S. Feng, M. Richard-Greenblatt, E. Hutson, S. Andrianus, L. J. Glaser, K.G. Rodino, J. Qian, D. Jayaraman, R.G. Collman, A. Glascock, F. D. Bushman, J.S. Lee, S. Cherry, A. Fausto, S.R. Weiss, H. Koo, P.M. Corby, A. Oceguera, U. O'Doherty, A.L. Garfall, D.T. Vogl, E.A. Stadtmauer, P. Wang, Clin. Chem. 68 (2021) 230.
[70] Y. Li, Z. Peng, N.J. Holl, M.R. Hassan, J.M. Pappas, C. Wei, O.H. Izadi, Y. Wang, X. Dong, C. Wang, Y.W. Huang, D. Kim, C. Wu, ACS Omega 6 (2021) 6643.
[71] H. Tavakoli, W. Zhou, L. Ma, Q. Guo, X. Li, Paper and Paper Hybrid Microfluidic Devices for Point-of-care Detection of Infectious Diseases, Wiley, 2020, p. 177.
[72] J. Li, P.B. Lillehoj, ACS Sens. 6 (2021) 1270.
[73] Q. Lin, D. Wen, J. Wu, L. Liu, W. Wu, X. Fang, J. Kong, Anal. Chem. 92 (2020) 9454.
[74] S.K. Katla, W. Zhou, H. Tavakoli, E.L.P. Méndez, X. Li, View 4 (2023) 20220053.
[75] J.H. Lee, P.K. Bae, H. Kim, Y.J. Song, S.Y. Yi, J. Kwon, J.S. Seo, J.M. Lee, H.S. Jo, S.M. Park, H.S. Park, K.S. Shin, S. Chung, Y.B. Shin, Biosens. Bioelectron. 191 (2021) 113406.
[76] J. Yang, V.M. Phan, C.K. Heo, H.V. Nguyen, W.H. Lim, E.W. Cho, H. Poo, T.S. Seo, Sensor. Actuator. B Chem. 380 (2023) 133331.
[77] S.T. Sanjay, G. Fu, M. Dou, F. Xu, R. Liu, H. Qi, X. Li, Analyst 140 (2015) 7062.
[78] M. Dou, S.T. Sanjay, M. Benhabib, F. Xu, X. Li, Talanta 145 (2015) 43.
[79] M. Dou, S.T. Sanjay, D.C. Dominguez, S. Zhan, X. Li, Chem. Commun. 53 (2017) 10886.
[80] D. Liu, Y. Wang, X. Li, M. Li, Q. Wu, Y. Song, Z. Zhu, C. Yang, Aggregate 3 (2022) e184.
[81] Y.J. Juang, S.K. Hsu, Polymers 14 (2022) 639.
[82] K.S. Rajsri, M.P. McRae, G.W. Simmons, N.J. Christodoulides, H. Matz, H. Dooley, A. Koide, S. Koide, J.T. McDevitt, Biosensors 12 (2022) 621.
[83] H. Han, C. Wang, X. Yang, S. Zheng, X. Cheng, Z. Liu, B. Zhao, R. Xiao, Sensor. Actuator. B Chem. 351 (2022) 130897.
[84] Y. Joung, K. Kim, S. Lee, B.S. Chun, S. Lee, J. Hwang, S. Choi, T. Kang, M.K. Lee, L. Chen, J. Choo, ACS Sens. 7 (2022) 3470.
[85] J. Li, L.T. Chu, H. Hartanto, G. Guo, L. Liu, J. Wu, M. Wu, C. Cui, G. Wang, W. Liu, H.K. Kwong, S. Wu, T.-H. Chen, Lab Chip 24 (2024) 2658.
[86] Y. Liu, J. Li, Z. Xiao, T. Wu, C. Zhou, J. Zhou, Small 20 (2023) e2309956.

[87] S. Liu, Y. Hou, Z. Li, C. Yang, G. Liu, ACS Sens. 8 (2023) 3520.
[88] Y. Zeng, X. Gan, Z. Xu, X. Hu, C. Hu, H. Ma, H. Tu, B. Chai, C. Yang, S. Hu, Y. Chai, Anal. Chim. Acta 1298 (2024) 342398.
[89] C. Ge, J. Feng, J. Zhang, K. Hu, D. Wang, L. Zha, X. Hu, R. Li, Talanta 236 (2022) 122847.
[90] Y. Huang, Q. Wu, J. Zhang, Y. Zhang, S. Cen, C. Yang, Y. Song, ACS Nano 17 (2023) 21973.
[91] L.F. Yang, N. Kacherovsky, N. Panpradist, R. Wan, J. Liang, B. Zhang, S. J. Salipante, B.R. Lutz, S.H. Pun, Anal. Chem. 94 (2022) 7278.
[92] G. Fu, S.T. Sanjay, M. Dou, X. Li, Nanoscale 8 (2016) 5422.
[93] G. Fu, S.T. Sanjay, W. Zhou, R.A. Brekken, R.A. Kirken, X. Li, Anal. Chem. 90 (2018) 5930.
[94] W. Zhou, G. Fu, X. Li, Anal. Chem. 93 (2021) 7754.
[95] G. Fu, W. Zhou, X. Li, Lab Chip 20 (2020) 2218.
[96] R. Chen, C. Ren, M. Liu, X. Ge, M. Qu, X. Zhou, M. Liang, Y. Liu, F. Li, ACS Nano 15 (2021) 8996.
[97] S. Ruantip, U. Pimpitak, S. Rengpipat, E. Pasomsub, C. Seepiban, O. Gajanandana, P. Torvorapanit, N. Hirankarn, P. Jaru-Ampornpan, S. Siwamogsatham, P. Pongpaibool, S. Siwamogsatham, N. Thongchul, S. Chaiyo, Sensor. Actuator. B, Chem 389 (2023) 133898.
[98] H. Shen, X. Chen, L. Zeng, X. Xu, Y. Tao, S. Kang, Y. Lu, M. Lian, C. Yang, Z. Zhu, Anal. Chem. 94 (2022) 8458.
[99] H. Wang, C. Yao, J. Fan, Y. He, Z. Wang, Biosens. Bioelectron. 237 (2023) 115508.
[100] W. Zhou, J. Sun, X. Li, Anal. Chem. 92 (2020) 14830.
[101] C. Carrell, I. Jang, J. Link, J.S. Terry, Z. Call, Y. Panraksa, O. Chailapakul, D. S. Dandy, B.J. Geiss, C.S. Henry, Anal. Methods 15 (2023) 2721.
[102] H.K. Oh, K. Kim, J. Park, H. Im, S. Maher, M.G. Kim, Biosens. Bioelectron. 205 (2022) 114094.
[103] Z. Wang, Z. Zheng, H. Hu, Q. Zhou, W. Liu, X. Li, Z. Liu, Y. Wang, Y. Ma, Lab Chip 20 (2020) 4255.
[104] A. Parandakh, O. Ymbern, W. Jogia, J. Renault, A. Ng, D. Juncker, Lab Chip 23 (2023) 1547.
[105] S. Kim, E. Yee, E.A. Miller, Y. Hao, D.M.Y. Tay, K.J. Sung, H. Jia, J.M. Johnson, M. Saeed, C.R. Mace, D. Yuksel Yurt, H.D. Sikes, ACS Appl. Mater. Interfaces 13 (2021) 38990.
[106] L. Ma, Y. Abugalyon, X. Li, Anal. Bioanal. Chem. 413 (2021) 4655.
[107] Y. Liu, Y. Tan, Q. Fu, M. Lin, J. He, S. He, M. Yang, S. Chen, J. Zhou, Biosens. Bioelectron. 176 (2021) 112920.
[108] J. Xu, W. Suo, Y. Goulev, L. Sun, L. Kerr, J. Paulsson, Y. Zhang, T. Lao, Small 17 (2021) e2104009.
[109] F. Wu, M. Mao, L. Cai, Q. Lin, X. Guan, X. Shi, L. Ma, ACS Biomater. Sci. Eng. 8 (2022) 3924.
[110] L.D. Xu, J. Zhu, S.N. Ding, Analyst 146 (2021) 5055.
[111] M. Feng, J. Chen, J. Xun, R. Dai, W. Zhao, H. Lu, J. Xu, L. Chen, G. Sui, X. Cheng, ACS Sens. 5 (2020) 2331.
[112] S. Li, F. Wang, B. Zhao, C. Wang, Z. Wang, Q. Wu, Anal. Chim. Acta 1279 (2023) 341844.
[113] H. Li, B. Zhu, B. Li, L. Chen, X. Ning, H. Dong, J. Liang, X. Yang, J. Dong, H. Ueda, Sci. Rep. 12 (2022) 15496.
[114] R. Gupta, P. Gupta, S. Wang, A. Melnykov, Q. Jiang, A. Seth, Z. Wang, J. J. Morrissey, I. George, S. Gandra, P. Sinha, G.A. Storch, B.A. Parikh, G.M. Genin, S. Singamaneni, Nat. Biomed. Eng. 7 (2023) 1556.
[115] Y. Zhang, Y. Chen, Y. He, Y. Li, X. Zhang, J. Liang, J. He, S. Lu, Z. Gao, J. Xu, Y. Tang, Talanta 255 (2023) 124200.
[116] Laboratory testing for coronavirus disease 2019 (ſCOVID-19)ſ in suspected human cases: interim guidance, 2, World Health Organization, 2020. March, https://iris.who.int/handle/10665/331329.
[117] Y. Zhou, Y. Chen, W. Liu, H. Fang, X. Li, L. Hou, Y. Liu, W. Lai, X. Huang, Y. Xiong, Sensor. Actuator. B Chem. 343 (2021) 130139.
[118] X. Duan, Y. Shi, X. Zhang, X. Ge, R. Fan, J. Guo, Y. Li, G. Li, Y. Ding, R.A. Osman, W. Jiang, J. Sun, X. Luan, G. Zhang, Biosens. Bioelectron. 199 (2022) 113883.
[119] Y. Liang, B.C. Buchanan, B. Khanthaphixay, A. Zhou, G. Quirk, M. Worobey, J. Y. Yoon, Biosens. Bioelectron. 229 (2023) 115221.
[120] W. Lee, H. Kim, P.K. Bae, S. Lee, S. Yang, J. Kim, Biosens. Bioelectron. 190 (2021) 113388.
[121] S. Kim, P. Akarapipad, B.T. Nguyen, L.E. Breshears, K. Sosnowski, J. Baker, J. L. Uhrlaub, J. Nikolich-Zugich, J.Y. Yoon, Biosens. Bioelectron. 200 (2022) 113912.
[122] Q. Lin, J. Zhang, L. Liu, J. Kong, X. Fang, ACS Omega 7 (2022) 38409.
[123] H.A. Al Lawati, Luminescence 28 (2013) 618.
[124] Y. Nie, Z. Liang, P. Wang, Q. Ma, X. Su, Anal. Chem. 93 (2021) 17086.
[125] X. Song, X. Ren, W. Zhao, L. Zhao, S. Wang, C. Luo, Y. Li, Q. Wei, Anal. Chem. 94 (2022) 12531.
[126] Y. Zhou, S. Xie, B. Liu, C. Wang, Y. Huang, X. Zhang, S. Zhang, Anal. Chem. 95 (2023) 3332.
[127] N.M. Kumar, P. Picchetti, C. Hu, L.M. Grimm, F. Biedermann, ACS Sens. 7 (2022) 2312.
[128] R. Wang, N. Yue, A. Fan, Analyst 145 (2020) 7488.
[129] L. Mou, Y. Zhang, Y. Feng, H. Hong, Y. Xia, X. Jiang, Anal. Chem. 94 (2022) 2510.
[130] J. Klupfel, S. Passreiter, N. Weidlein, M. Knopp, M. Ungerer, U. Protzer, P. Knolle, O. Hayden, M. Elsner, M. Seidel, Anal. Chem. 94 (2022) 2855.
[131] Z. Zheng, L. Wu, L. Li, S. Zong, Z. Wang, Y. Cui, Talanta 188 (2018) 507.
[132] R. Panneerselvam, H. Sadat, E.M. Höhn, A. Das, H. Noothalapati, D. Belder, Lab Chip 22 (2022) 665.
[133] B. Gosselin, M. Retout, R. Dutour, L. Troian-Gautier, R. Bevernaegie, S. Herens, P. Lefevre, O. Denis, G. Bruylants, I. Jabin, Anal. Chem. 94 (2022) 7383.
[134] J. Li, P. Liang, T. Zhao, G. Guo, J. Zhu, C. Wen, J. Zeng, Anal. Bioanal. Chem. 415 (2023) 545.
[135] N. Choi, H. Dang, A. Das, M.S. Sim, I.Y. Chung, J. Choo, Biosens. Bioelectron. 164 (2020) 112326.
[136] H. Liu, E. Dai, R. Xiao, Z. Zhou, M. Zhang, Z. Bai, Y. Shao, K. Qi, J. Tu, C. Wang, S. Wang, Sensor. Actuator. B Chem. 329 (2021) 129196.
[137] S. Park, C. Su Jeon, N. Choi, J.I. Moon, K. Min Lee, S. Hyun Pyun, T. Kang, J. Choo, Chem. Eng. J. 446 (2022) 137085.
[138] S. Srivastav, A. Dankov, M. Adanalic, R. Grzeschik, V. Tran, S. Pagel-Wieder, F. Gessler, I. Spreitzer, T. Scholz, B. Schnierle, O.E. Anastasiou, U. Dittmer, S. Schlucker, Anal. Chem. 93 (2021) 12391.
[139] P. Liang, Q. Guo, T. Zhao, C.Y. Wen, Z. Tian, Y. Shang, J. Xing, Y. Jiang, J. Zeng, Anal. Chem. 94 (2022) 8466.
[140] S. Chen, L. Meng, L. Wang, X. Huang, S. Ali, X. Chen, M. Yu, M. Yi, L. Li, X. Chen, L. Yuan, W. Shi, G. Huang, Sensor. Actuator. B Chem. 348 (2021) 130706.
[141] R. Funari, K.Y. Chu, A.Q. Shen, Biosens. Bioelectron. 169 (2020) 112578.
[142] I.C. Samper, C.J. McMahon, M.S. Schenkel, K.M. Clark, W. Khamcharoen, L.B. R. Anderson, J.S. Terry, E.N. Gallichotte, G.D. Ebel, B.J. Geiss, D.S. Dandy, C. S. Henry, Anal. Chem. 94 (2022) 4712.
[143] W. Teixeira, Y. Pallás-Tamarit, A. Juste-Dolz, A. Sena-Torralba, R. Gozalbo-Rovira, J. Rodríguez-Díaz, D. Navarro, J. Carrascosa, D. Gimenez-Romero, Á. Maquieira, S. Morais, Biosensors, Bioelectron. 213 (2022) 114454.
[144] N.M. Kilic, S. Singh, G. Keles, S. Cinti, S. Kurbanoglu, D. Odaci, Biosensors 13 (2023) 622.
[145] P. Kannan, G. Maduraiveeran, Biosensors 13 (2023) 542.
[146] R.M. Silva, A.D. da Silva, J.R. Camargo, B.S. de Castro, L.M. Meireles, P.S. Silva, B.C. Janegitz, T.A. Silva, Biosensors 13 (2023) 453.
[147] S. Srikanth, U.S. Jayapiriya, S.K. Dubey, A. Javed, S. Goel, iScience 25 (2022) 105388.
[148] I.C. Samper, A. Sanchez-Cano, W. Khamcharoen, I. Jang, W. Siangproh, E. Baldrich, B.J. Geiss, D.S. Dandy, C.S. Henry, ACS Sens. 6 (2021) 4067.
[149] R. Siavash Moakhar, C. Del Real Mata, M. Jalali, H. Shafique, A. Sanati, J. de Vries, J. Strauss, T. AbdElFatah, F. Ghasemi, M. McLean, I.H. I, Y. Lu, S.G. Yedire, S.S. Mahshid, M.A. Tabatabaiefar, C. Liang, S. Mahshid, Adv. Sci. 9 (2022) e2204246.
[150] V. Mazzaracchio, M. Rios Maciel, T. Porto Santos, K. Toda-Peters, A.Q. Shen, Small, 2023 e2207731.
[151] D. Najjar, J. Rainbow, S. Sharma Timilsina, P. Jolly, H. de Puig, M. Yafia, N. Durr, H. Sallum, G. Alter, J.Z. Li, X.G. Yu, D.R. Walt, J.A. Paradiso, P. Estrela, J. J. Collins, D.E. Ingber, Nat. Biomed. Eng. 6 (2022) 968.
[152] M.A. Ali, C. Hu, S. Jahan, B. Yuan, M.S. Saleh, E. Ju, S.J. Gao, R. Panat, Adv. Mater. 33 (2021) e2006647.
[153] G. Fu, Y. Zhu, W. Wang, M. Zhou, X. Li, ACS Sens. 4 (2019) 2481.
[154] G. Fu, Y. Zhu, K. Xu, W. Wang, R. Hou, X. Li, Anal. Chem. 91 (2019) 13290.
[155] G. Fu, R. Hou, X. Mou, X. Li, Anal. Chem. 93 (2021) 15105.
[156] G. Fu, X. Li, W. Wang, R. Hou, Biosens. Bioelectron. 170 (2020) 112646.
[157] M. Wu, S. Wu, G. Wang, W. Liu, L.T. Chu, T. Jiang, H.K. Kwong, H.L. Chow, I.W. S. Li, T.-H. Chen, Sci. Adv. 8 (2022) eabn6064.
[158] G. Fu, S.T. Sanjay, M. Dou, X. Li, Nanoscale 8 (2016) 5422.
[159] W. Zhou, K. Hu, S. Kwee, L. Tang, Z. Wang, J. Xia, X. Li, Anal. Chem. 92 (2020) 2739.
[160] L. Lu, X. Hu, R. Zeng, Q. Lin, X. Huang, Q. Wei, D. Tang, D. Knopp, Biosens. Bioelectron. 230 (2023) 115267.
[161] Z. Yu, C. Qiu, L. Huang, Y. Gao, D. Tang, Anal. Chem. 95 (2023) 4212.
[162] Y. Liu, L. Zhan, J.W. Shen, B. Baro, A. Alemany, J. Sackrison, O. Mitja, J. C. Bischof, ACS Appl. Nano Mater. 4 (2021) 13826.
[163] X. Wei, T. Tian, S. Jia, Z. Zhu, Y. Ma, J. Sun, Z. Lin, C.J. Yang, Anal. Chem. 88 (2016) 2345.
[164] K. Maejima, Y. Hiruta, D. Citterio, Anal. Chem. 92 (2020) 4749.
[165] M. Rahbar, A.R. Wheeler, B. Paull, M. Macka, Anal. Chem. 91 (2019) 8756.
[166] C. Qian, J. Li, Z. Pang, H. Xie, C. Wan, S. Li, X. Wang, Y. Xiao, X. Feng, Y. Li, P. Chen, B.F. Liu, Talanta 258 (2023) 124466.
[167] P. Akarapipad, K. Kaarj, L.E. Breshears, K. Sosnowski, J. Baker, B.T. Nguyen, C. Eades, J.L. Uhrlaub, G. Quirk, J. Nikolich-Zugich, M. Worobey, J.Y. Yoon, Biosens. Bioelectron. 207 (2022) 114192.
[168] H. Tavakoli, S. Mohammadi, X. Li, G. Fu, X. Li, TrAC, Trends Anal. Chem. 157 (2022) 116806.
[169] K.S. Prasad, Y. Abugalyon, C. Li, F. Xu, X. Li, Analyst 145 (2020) 5113.
[170] M. Lv, W. Zhou, H. Tavakoli, C. Bautista, J. Xia, Z. Wang, X. Li, Biosens. Bioelectron. 176 (2021) 112947.
[171] Q. Jin, L. Ma, W. Zhou, Y. Shen, O. Fernandez-Delgado, X. Li, Chem. Sci. 11 (2020) 2915.
[172] K. Hu, L. Ma, Z. Wang, O. Fernandez-Delgado, Y.E. Garay, J.A. Lopez, X. Li, ACS Sustainable Chem. Eng. 10 (2022) 10579.
[173] Y. Gong, Y. Zheng, B. Jin, M. You, J. Wang, X. Li, M. Lin, F. Xu, F. Li, Talanta 201 (2019) 126.
[174] X. Xu, X. Wang, J. Hu, Y. Gong, L. Wang, W. Zhou, X. Li, F. Xu, Electrophoresis 40 (2019) 914.
[175] X. Xu, A. Akay, H. Wei, S. Wang, B. Pingguan-Murphy, B. Erlandsson, X. Li, W. Lee, J. Hu, L. Wang, F. Xu, Proc. IEEE 103 (2015) 236.
[176] H. Tavakoli, J. Sun, X. Li, IEEE BioSensors Conf. (2023) 1.
[177] W. Zhou, K. Hu, S. Kwee, L. Tang, Z. Wang, J. Xia, X. Li, Anal. Chem. 92 (2020) 2739.
[178] J. Zhang, H. Xing, Y. Lu, Chem. Sci. 9 (2018) 3906.

[179] T. Lan, J. Zhang, Y. Lu, Biotechnol. Adv. 34 (2016) 331.
[180] G. Henao-Pabon, N. Gao, K.S. Prasad, X. Li, Biosensors 13 (2023) 566.
[181] I. Jang, D.B. Carrão, R.F. Menger, A.R. Moraes de Oliveira, C.S. Henry, ACS Sens. 5 (2020) 2230.
[182] M. Dou, N. Macias, F. Shen, J. Dien Bard, D.C. Domínguez, X. Li, EClinicalMedicine 8 (2019) 72.